BBA - Molecular and Cell Biology of Lipids 1870 (2025) 159574

Contents lists available at ScienceDirect

BBA - Molecular and Cell Biology of Lipids

journal homepage: www.elsevier.com/locate/bbalip

How the liver transcriptome and lipid composition influence the progression of nonalcoholic fatty liver disease to hepatocellular carcinoma in a murine model

Marvin Leopold [a,d,1], Paola Berenice Mass-Sanchez [b,1], Marinela Krizanac [b], Paula Štancl [c], Rosa Karlić [c], Patricia Prabutzki [a], Victoria Parafianczuk [a], Jürgen Schiller [a], Anastasia Asimakopoulos [b], Kathrin M. Engel [a,*], Ralf Weiskirchen [b,*]

[a] Institute for Medical Physics and Biophysics, Leipzig University, Faculty of Medicine, 04107 Leipzig, Germany
[b] Institute of Molecular Pathobiochemistry, Experimental Gene Therapy and Clinical Chemistry (IFMPEGKC), RWTH University Hospital Aachen, 52074 Aachen, Germany
[c] Bioinformatics Group, Division of Molecular Biology, Department of Biology, Faculty of Science, University of Zagreb, Zagreb, Croatia
[d] Klinik für Neurologie, Sana Klinikum Borna, 04552 Borna, Germany

ARTICLE INFO

Keywords:
Nonalcoholic fatty liver disease
Hepatocellular carcinoma
Fatty acid metabolism
Lipidomics

ABSTRACT

The incidence of nonalcoholic fatty liver disease (NAFLD) has been steadily increasing in Western society in recent years and has been recognized as a risk factor for the development of hepatocellular carcinoma (HCC). However, the molecular mechanisms underlying the progression from NAFLD to HCC are still unclear, despite the use of suitable mouse models. To identify the transcriptional and lipid profiles of livers from mice with NAFLD-HCC, we induced both NAFLD and NAFLD-HCC pathologies in C57BL/6J mice and performed RNA-sequencing (RNA-seq) and targeted lipidomic analysis. Our RNA-seq analysis revealed that the transcriptional signature of NAFLD in mice is characterized by changes in inflammatory response and fatty acid metabolism. Moreover, the signature of NAFLD-HCC is characterized by processes typically observed in cancer, such as epithelial to mesenchymal transition, angiogenesis and inflammatory responses. Furthermore, we found that the diet used in this study inhibited cholesterol synthesis in both models. The analysis of lipid composition also showed a significant impact of the provided diet. Therefore, our study supports the idea that a Western diet (WD) affects metabolic processes and hepatic lipid composition. Additionally, the combination of a WD with the administration of a carcinogen drives the progression from NAFLD to HCC.

Abbreviations: Acly, ATP citrate lyase; Ccl20, C-C motif chemokine ligand 20; CD36, cluster of differentiation 36; CL, cardiolipin; DAG, diacylglycerol; Dgat1, diacylglycerol acyltransferase-1; DEG, differentially expressed gene; DMBA, 7,12-dimethylbenz[*a*]anthracene; Egr1, early growth response protein 1; EMT, epithelial to mesenchymal transition; ESI, electrospray ionization; FA, fatty acid; Fabp2, fatty acid-binding protein 2; Fasn, fatty acid synthase; HCC, hepatocellular carcinoma; HE, hematoxylin and eosin; HFD, high-fat diet; Hmgcr, 3-hydroxy-3-methylglutaryl-CoA reductase; HNF1, hepatocyte nuclear factor; Igfbp3, insulin like growth factor binding protein 3; Lgals1, galectin 1; Lpl, lipoprotein lipase; Marcks, myristoylated alanine-rich protein kinase C substrate; MS, mass spectrometry; mTORC1, mammalian target of rapamycin complex 1; NAFLD, nonalcoholic fatty liver disease; NF-κB, nuclear factor kappa-light-chain-enhancer of activated B cells; Nfkbie, NF-κB inhibitor epsilon; NR1l2, nuclear receptor subfamily 1 group i member 2; PC, phosphatidylcholine; PE, phosphatidylethanolamine; PI, phosphatidylinositol; Plod 2, procollagen-lysine-2-oxoglutarate 5-dioxygenase 2; SM, sphingomyelin; Spp1, secreted phosphoprotein 1; Sqle, squalene epoxidase; TAG, triacylglycerol; Tal1, T-cell acute lymphocytic leukemia 1; TFEA, transcriptional factors enrichment analysis; TLC, thin-layer chromatography; WD, Western diet.

* Corresponding authors.
E-mail addresses: marvin.leopold@medizin.uni-leipzig.de (M. Leopold), beremass@gmail.com (P.B. Mass-Sanchez), mkrizanac@ukaachen.de (M. Krizanac), pstancl@mail.bioinfo.hr (P. Štancl), rosa@bioinfo.hr (R. Karlić), patricia.prabutzki@medizin.uni-leipzig.de (P. Prabutzki), juergen.schiller@medizin.uni-leipzig.de (J. Schiller), kathrin.engel@medizin.uni-leipzig.de (K.M. Engel), rweiskirchen@ukaachen.de (R. Weiskirchen).
[1] These authors contributed equally to this work.

https://doi.org/10.1016/j.bbalip.2024.159574
Received 4 June 2024; Received in revised form 28 October 2024; Accepted 29 October 2024
Available online 5 November 2024
1388-1981/© 2024 The Author(s). Published by Elsevier B.V. This is an open access article under the CC BY license (http://creativecommons.org/licenses/by/4.0/).

1. Introduction

Nonalcoholic fatty liver disease (NAFLD) is a highly prevalent pathology affecting approximately 30–32 % of the European population [1,2]. In its early stages, NAFLD is characterized by the accumulation of fat inside hepatocytes, known as non-alcoholic fatty liver (NAFL). However, this often leads to inflammation-driven scarred remodeling of liver tissue known as non-alcoholic steatohepatitis (NASH), which can ultimately result in liver cirrhosis or primary hepatocellular carcinoma (HCC) [3]. Additionally, NAFLD has been shown to increase the risk of certain extrahepatic malignancies, such as gastrointestinal and gynecological cancers [4]. Since various conditions can lead to NAFLD and alcohol intake was considered an arbitrary exclusion criterion for diagnosis, an alternative, more inclusive nomenclature was suggested a few years ago: metabolic dysfunction-associated fatty liver disease (MAFLD) [5]. Despite the significant burden on global health and the expanding knowledge of its underlying pathophysiologies, there is still a lack of knowledge about NAFLD's origins [6]. According to the 'parallel multiple hits' theory, fatty liver formation is worsened by a variety of factors that ultimately contribute to the development of primary liver cancer. Factors such as lipid oxidation, insulin resistance, hormone alterations from adipose tissue, nutritional factors, gut microbiota and genetic and epigenetic factors have been extensively studied in recent years to uncover the mechanisms involved in NAFLD development and progression to HCC [7,8]. Although HCC is a multifactorial malignancy, it is predicted that its incidence will significantly increase due to the epidemic levels of obesity [9].

To date, several murine models of NAFLD have been developed to study the mechanisms involved in the progression of the disease to HCC, but these models only partially mimic the human disease [10].

It has been reported that mice fed a Western diet (WD), enriched in high-fat and high-fructose, exhibit a metabolism and histological phenotype that resembles human NAFLD [11]. However, there have been only a few studies in mice that accurately mimic the progression from NAFLD to HCC. Previous research has shown that a single dose of the carcinogen 7,12-Dimethylbenz[*a*]anthracene (DMBA) given during postnatal age, along with a high-fat diet (HFD), promotes the development of hepatic tumors that share many characteristics with human HCC [12]. In this model, DMBA causes an oncogenic mutation in the H-ras gene, and when combined with obesity, HCC develops. However, DMBA alone is not sufficient to cause liver cancer [12]. Another study, following a similar procedure, found that HCC development was only observed in DMBA-treated mice that were fed HFD for 40 weeks. Interestingly, hyperglycemia did not have any tumor-promoting effects during HCC development in this model [13]. Furthermore, other studies have made slight modifications to the original model and demonstrated that liver tumorigenesis is dependent on the implementation of a HFD [14,15].

Recently, a cell line derived from a DMBA-HFD model was obtained [14]. When cultured, these cells lose expression of the classical liver marker albumin, but maintain expression of the transcriptional factor hepatocyte nuclear factor 1 (HNF1). Additionally, high levels of the epithelial–mesenchymal-transition (EMT) markers, twist-related protein 1 (Twist1) and snail family transcriptional repressor 1 (Snail1) were observed. These findings indicate that this model mimics several features of HCC observed in humans and that risk factors such as obesity play a major role in liver tumorigenesis.

To our knowledge, no transcriptomic and lipidomic characterization of the DMBA-based NAFLD-HCC model and the NAFLD model that relies on a WD supplemented with glucose/fructose has been performed. Therefore, we analyzed both profiles in each model using RNA-sequencing (RNA-seq) and lipidomics. Our results revealed significant differences in the transcriptomic profile between NAFLD mice and NAFLD-HCC mice. Specifically, differences were found in the activation of inflammatory pathways and alterations in pathways associated with cholesterol homeostasis and lipid metabolism. On a cellular level, lipid analyses confirmed the incorporation of fatty acids (FA) from the respective diet into the liver (phospho)lipids.

Collectively, these data indicate that DMBA acts as an oncogenic agent that triggers the activation of inflammatory pathways. However, its subsequent carcinogenic effects are only promoted when mice are simultaneously fed with a high-calorie WD.

2. Materials and methods

2.1. Animals and induction of hepatic tumors

Male wild type (WT) C57BL/6J mice were housed at the Institute for Laboratory Animal Science at the RWTH University Hospital Aachen. Males were selected due to their higher susceptibility to developing fibrosis [16]. Due to conflicting evidence regarding the impact of thermoneutral housing conditions on HFD-NAFLD mouse models, we opted to use established in-house housing protocols [17–19]. In summary, mice were maintained under controlled conditions of 20 °C temperature, 50 % humidity, and a 12:12 h light-dark cycle. They were treated as previously described with slight modifications [14]. Briefly, 4 to 5-day-old pups were either treated with 50 µL of 0.5 % DMBA (dissolved in acetone) or acetone (vehicle) (Fig. 1). After the weaning period, the mice were separated into different groups and assigned to either a normal diet (ND, V1534, ssniff Spezialdiäten GmbH, Soest, Germany) containing 9 kcal% fat or a HFD (#D17010102, Research Diets, Inc., New Brunswick, NJ, USA) containing 40 kcal% fat. The mice on the HFD had ad libitum access to water supplemented with fructose 55 % (w/v) and glucose 45 % (w/v) (WD), which was changed every two weeks. The diet was given for 30 w. The mice treated with acetone alone represented the NAFLD model, while the mice treated with DMBA were used as the NAFLD-HCC model. At the end of the 30 w, all mice were sacrificed under inhalation anesthesia with isoflurane (Forene, Abbott, Wiesbaden, Germany). All animals used in this study received humane care, and all protocols were in full compliance with the guidelines for animal experimentation and were approved by the institutional German Animal Care Committee (LANUV, Recklinghausen, Germany, permit Az.:81–02.04.2019.A366).

2.2. Liver histology

After dissection, liver sections were fixed in 4 % paraformaldehyde (Otto Fischar GmbH & Co KG, Saarbrücken, Germany) for 24 h. Dehydration was performed using a fully automated tissue processor at the Interdisciplinary Center for Clinical Research (IZKF) at RWTH University Hospital Aachen. The samples were then embedded in paraffin and cut into slices with a thickness of 5 µm. Hematoxylin and eosin (HE) and Sirius red staining were carried out using standard procedures, and the slides were scanned with the NanoZoomer SQ digital slide scanner C13140-21 (Hamamatsu Photonics, Hamamatsu, Japan). The visualization of the slides was done using the NDP.view2 viewer (ver. 2.9.25)

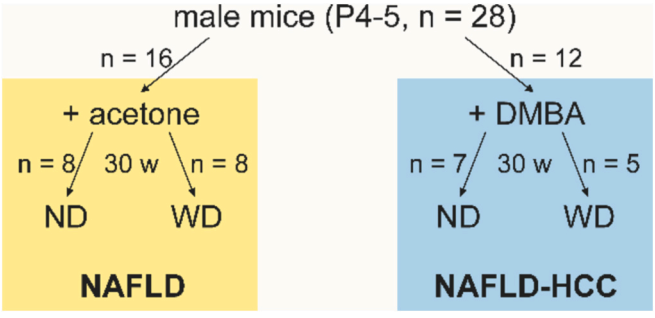


Fig. 1. Schematic representation of the animal treatment. Four to five-day-old pups were either treated with DMBA or acetone as the vehicle. They were then fed either a normal diet (ND) or a Western diet (WD) for 30 weeks. Male mice were exclusively used due to their limited diversity.

software (#U12388–01, Hamamatsu Photonics).

2.3. RNA isolation and RT-qPCR

Total RNA was extracted using phenol-chloroform and precipitated with isopropanol. Subsequent purification was carried out using the PureLink® RNA Mini Kit (Invitrogen, Thermo Fisher Scientific, Darmstadt, Germany) according to the manufacturer's instructions. First-strand cDNA was synthesized from 1 μg RNA using SuperScript II reverse transcriptase and random hexamers (Thermo Fisher). For quantitative real-time PCR (RT-qPCR), the reactions were performed using Universal SYBR Green Super Mix reagent (Bio-Rad, Hercules, CA, USA) supplemented with 2 μM of forward and reverse primers and 5 ng of cDNA. The thermal cycler (7300 Real-Time PCR, Applied Biosystems, Waltham, MA, USA) was programmed as follows: 2 s at 50 °C, denaturation for 10 min at 95 °C, followed by 40 cycles of 15 s at 95 °C and 1 min at 60 °C. Values were normalized to the expression of the housekeeping gene glyceraldehyde 3-phosphate dehydrogenase (*Gapdh*). Relative mRNA expression was calculated using the $2^{-\Delta\Delta CT}$ method [20]. The primers used in this study are listed in Table S1.

2.4. RNA sequencing library preparation and analysis

Three randomly chosen biological replicates were used for each group. cDNA libraries were produced using 36× Colibri 3′ mRNA Library Preparation kit (Invitrogen) with an input of 500 ng of total RNA and 1 % denatured and diluted PhiX. The library was prepared as described [21]. Quality control was performed with FastQC v0.11.9. Reads were mapped to the mouse reference genome (mm10.GRCm38.GCA_000001635.2) using STAR [22] (version 2.7.3a) with the following settings: –outFilterScoreMinOverLread 0.25 –outFilterMatchNminOverLread 0.25 –alignSoftClipAtReferenceEnds "No" to optimize short read mapping. Only uniquely mapped reads were counted over gene features annotated from Ensembl (Mus_musculus.GRCm38.100.) using featureCounts [23] (version 2.0.0) with parameter –primary. Differential expression analysis was performed on each pairwise comparison of genotype, treatment and diet. Rlog transformed counts (rlog) were used for principal components analysis and average clustering of samples based on Euclidean distance using the pheatmap function from the R pheatmap package (version 1.0.12) [24]. The DESeq2 package (version 1.34.0) [25] in R was used to compute statistical fold changes using the LFC shrinkage apeglm package (version 1.16.0) [26]. Differentially expressed genes (DEG) were considered statistically differentially expressed with a false discovery rate (FDR)-adjusted p value < 0.05 and a log2-fold change >1. The online tool ShinyGO [27] was used to analyze the Kyoto Encyclopedia of Genes and Genomes (KEGG) pathways of the DEG constituting the NAFLD and NALFD-HCC transcriptional signatures. Enrichr RRID:SCR_001575 [28–30] was used to determine the pathways in which the given DEG list was enriched. The database used for the comparison corresponds to MSigDBHallmark 2020 [31,32]. This database encompasses the collection of "hallmark" gene sets derived from multiple "founder" sets that convey a specific biological state or process and display coherent expression [32]. Filtering of the data was performed manually by selecting pathways with a FDR < 0.05. For the transcriptional factor enrichment analysis (TFEA) with ChEA3, filtering was performed by selecting only data based on the literature and experiments performed in the livers of mice. Heatmaps were plotted using SRplot [33], an online platform for data analysis and visualization.

2.5. Lipid analysis

2.5.1. Lipid extraction

Liver samples and 100 mg of chow from the different diets were homogenized in 500 μL of methanol using the CKMix Tissue Homogenizing Kit and a Precellys tissue homogenizer (both from Bertin Technologies, Montigny-le-Bretonneux, France). Lipids from the homogenates were extracted in glass vials by adding 1.5 mL each of chloroform and methanol in a 1:1 ratio [34]. The mixture was then mixed for 30 min at 700 rpm and room temperature using a horizontal shaker. After that, 1.5 mL of water was added, and the samples were shaken for another 10 min. Phase separation was achieved by centrifugation at 3500 rpm and 20 °C for 7 min. One mL of the lower (organic) phase was withdrawn using a glass syringe and the lipid extraction process was repeated by adding 1 mL of chloroform, vigorously shaking, and centrifugation. The organic phase was once again withdrawn and combined with the first one. After evaporation to dryness, the lipids were dissolved in 100 μL of chloroform.

2.5.2. Thin-layer chromatography

Ten μl of each liver lipid sample were automatically sprayed onto a normal phase high-performance thin-layer chromatography (HPTLC) silica gel 60 plate (Merck KGaA, Darmstadt, Germany) using a CAMAG® Linomat 5 semi-automatic sample application system (CAMAG, Berlin, Germany). Polar lipids were separated by chloroform/ethanol/water/triethylamine (30:35:7:35, by volume), and apolar lipids were separated by *n*-hexane/diethyl ether/glacial acetic acid (80:15:1, by volume) as the mobile phases. The plates were developed to 0.2 cm from the upper end of the plate. Then, the plates were dipped into a 50 mg/L primuline solution (acetone/water 80:20, v/v, Sigma-Aldrich, Taufkirchen, Germany). Lipids were detected as colored spots upon illumination with UV light (366 nm) and marked with a pencil.

2.5.3. Characterization of lipid species by mass spectrometry

Liver lipids were eluted automatically using a Plate Express™ TLC plate reader (Advion, Ithaca, NY, USA) with methanol as the solvent. Methanolic extracts were then directly infused into an electrospray-ionization ion trap (ESI-IT) mass spectrometer.

The dietary lipids were not separated but instead analyzed using direct infusion ESI-IT mass spectrometry (MS).

ESI-IT MS was performed on an Amazon SL mass spectrometer (Bruker Daltonics GmbH, Bremen, Germany) under the following conditions: spray voltage of 4.5 kV, end plate offset of 500 V, nebulizer gas at 7.2 psi, drying gas (N_2) at a flow rate of 3 L/min, capillary temperature of 200 °C, flow rate of 3 μL/min, and sheath gas (He) flow rate of 25 a.u.. The spectra of liver lipids were recorded in either the positive or negative ion mode, depending on the lipid class, with enhanced resolution. Spectra for dietary lipids were recorded in alternating mode. Data were acquired using Trap Control software and analyzed using Data Analysis version 4.1 (Bruker Daltonics GmbH, Bremen, Germany).

2.5.4. Lipid data analysis

For the analysis of quantitative data, we used relative peak intensities. Relative values were expressed as ratios of the intensity of the respective lipid to the total intensity of all compounds within the corresponding lipid class. We performed the relative quantitative data analysis using Microsoft Excel 2016. Statistical analysis was conducted using GraphPad Prism® 8.4.3 (GraphPad Software, Inc.) and the R Statistical Software [35] (v4.3.0, R Core Team 2021). Graphical representations were generated using GraphPad Prism® 8.4.3, Corel DRAW 2020 22.0 (Corel corporation) and the Tidyverse R (version 2.0.0) [36], and the ggplot2 R package (version 3.4.3) [37].

3. Results

3.1. Implementation of a Western diet causes NAFLD and liver tumorigenesis in mice

The implementation of HFD is well documented to cause weight gain in rodent models [38,39]. In our experimental setup, WT mice were either treated once with acetone followed a ND (control group) or a WD (NAFLD model) feeding for 30 w. Alternatively, they were treated once with DMBA dissolved in acetone followed by a ND (control group) or a WD (NAFLD-HCC model) feeding for 30 w.

In both models, we first evaluated the initial and final weights of the animals. The results indicate that after the 30 w of diet, animals fed with the WD showed a significant increase in body weight compared to littermates fed a ND (Fig. 2A, F). The initiation of HCC by DMBA resulted in early death of two WD-fed mice, which were therefore excluded from the study. To evaluate the histopathological features of the liver, paraffin sections were stained with HE and Sirius Red. The latter stains collagen and was used to observe the level of fibrosis in the livers. Animals fed with a ND showed no anomalies in the liver, regardless of whether they were treated with acetone or the carcinogen as assessed in HE stain (Fig. 2B, G). In contrast, WD-fed mice developed classical features of hepatic steatosis, such as fat accumulation and fibrosis (Fig. 2D, E, I, J). Moreover, only the simultaneous treatment with the carcinogen and WD induced the development of hepatic tumors. Sirius Red staining further revealed that only WD-fed animals accumulated collagen deposits.

3.2. NALFD and NAFLD-HCC mice differ in their transcriptional signature

To understand the transcriptional reprogramming induced by the diet and treatments, RNA seq was performed.

First, pairwise differences in mice treated with acetone and either subjected to ND or WD (NAFLD model) were analyzed. The pairwise analysis revealed 532 DEG (Fig. 3A). Among these, 422 transcripts showed increased expression in the WD group compared to the ND group, while 110 showed decreased expression. For the upregulated genes, functional annotation of KEGG pathways revealed an increase in several processes related to lipid metabolism, such as cholesterol metabolism, glycerolipid metabolism and FA processing (Fig. 3B). A subsequent enrichment analysis showed that DEG were involved in pathways related to inflammatory-mediated response and FA metabolism (Fig. 3B). Regarding the downregulated genes, functional annotation of KEGG, revealed changes in metabolism homeostasis, while cholesterol metabolism and steroid (hormone) biosynthesis were found to be enriched (Fig. 3C).

In the case of mice treated with DMBA (NAFLD-HCC model), a

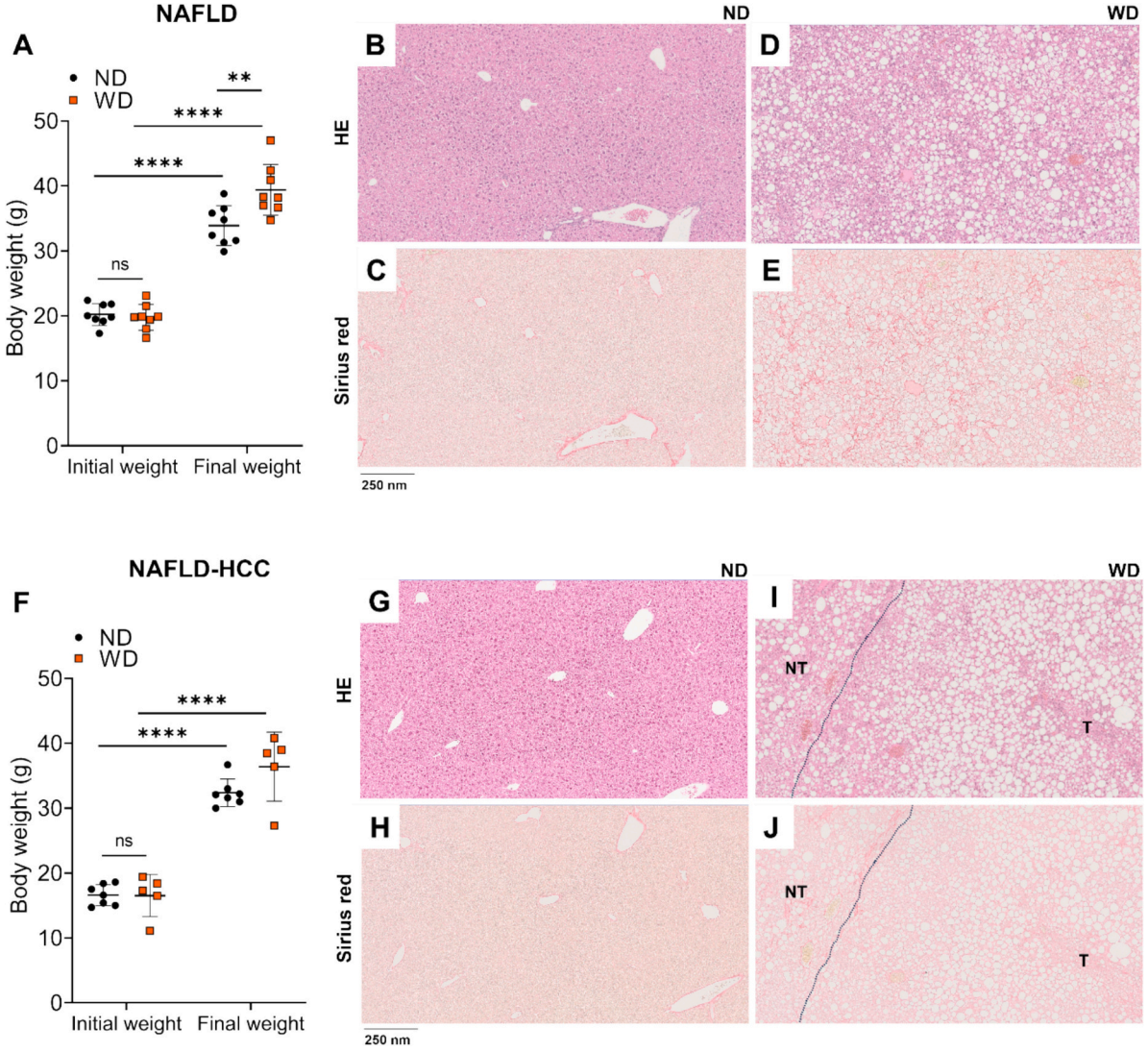


Fig. 2. Implementation of a Western diet (WD) induces lipid accumulation and fibrosis development in an NAFLD and NAFLD-HCC model. (A, F) Measurements of the initial and final body weights of mice subjected to the NAFLD (ND, $n = 8$; WD, $n = 8$) or the NAFLD-HCC model (ND, $n = 7$; WD, $n = 5$). (B–E, G–J) Representative liver sections of mice from (A, F) were stained with HE or Sirius Red. Digital zoom of 10× was used to create the images. Data represents mean ± SD. All data was analyzed by two-way ANOVA using Tukey post-hoc test. $^{**}p < 0.01$, $^{****}p < 0.0001$. HE, hematoxylin eosin; ND, normal diet; ns, not significant. (For interpretation of the references to color in this figure legend, the reader is referred to the web version of this article.)

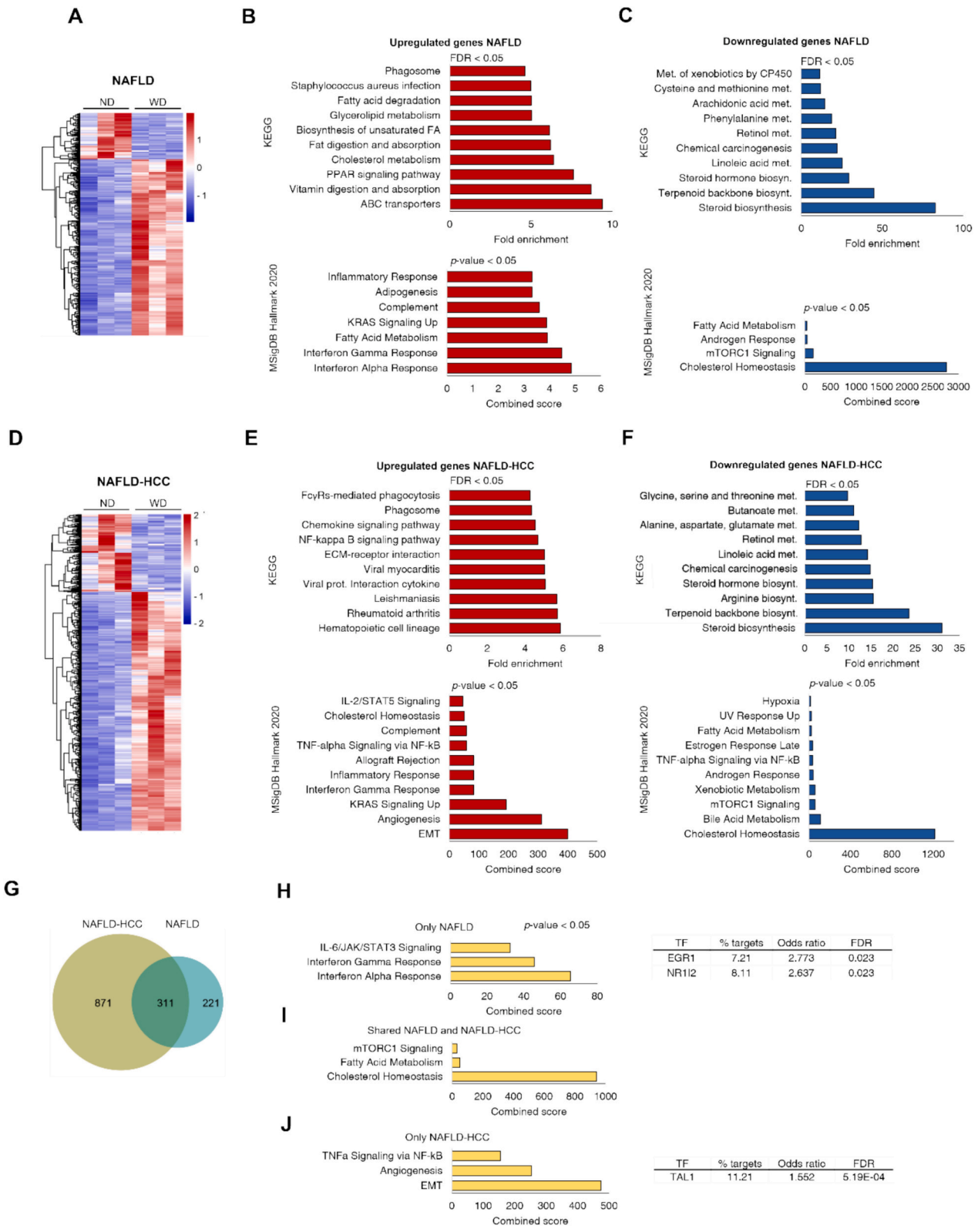


Fig. 3. RNA-seq data analyses of the NAFLD and NAFLD-HCC models. (A–C) Analysis of the NAFLD model. (A) Heatmap showing the 532 differentially expressed genes (DEG) in acetone-treated mice fed with a normal diet (ND) and Western diet (WD). Functional annotation analysis and enrichment analysis of the (B) upregulated and (C) downregulated DEG categorized in KEGG pathways and hallmark gene sets from the molecular signatures database (MsigDB). (D–F) Analysis of the NAFLD-HCC model. (D) Heatmap showing the 1182 DEG in wild-type (WT) DMBA-treated mice fed with ND and WD. Functional annotation analysis and enrichment analysis of the (E) upregulated and (F) downregulated DEG. (G) Venn diagram showing the overlapping DEG in the NAFLD and NAFLD-HCC models. (H) Enrichment analysis and transcription factor enrichment analysis (TFEA) on the DEG exclusively found in the NAFLD model. (I) Enrichment analysis of the overlapping genes between the two models. (J) Enrichment analysis and TFEA of the DEG exclusively found in the NAFLD-HCC model. For all analyses a false discovery rate (FDR)-adjusted p value of <0.05 and a log2-fold change >1 were used. $n = 3$ per group.

pairwise comparison of ND and WD revealed changes in 1182 DEG, out of which 892 were upregulated and 290 were downregulated (Fig. 3D). Among the upregulated genes, functional annotation analysis of KEGG, retrieved pathways associated with immune response. Additionally, there was an enrichment of processes characteristic of malignant transformation, such as EMT, angiogenesis, upregulation of KRAS signaling, and cholesterol homeostasis (Fig. 3E). On the other hand, functional annotation of KEGG showed that the downregulated genes were mostly involved in processes related to metabolism homeostasis. Enrichment analysis indicated that the set of downregulated genes was

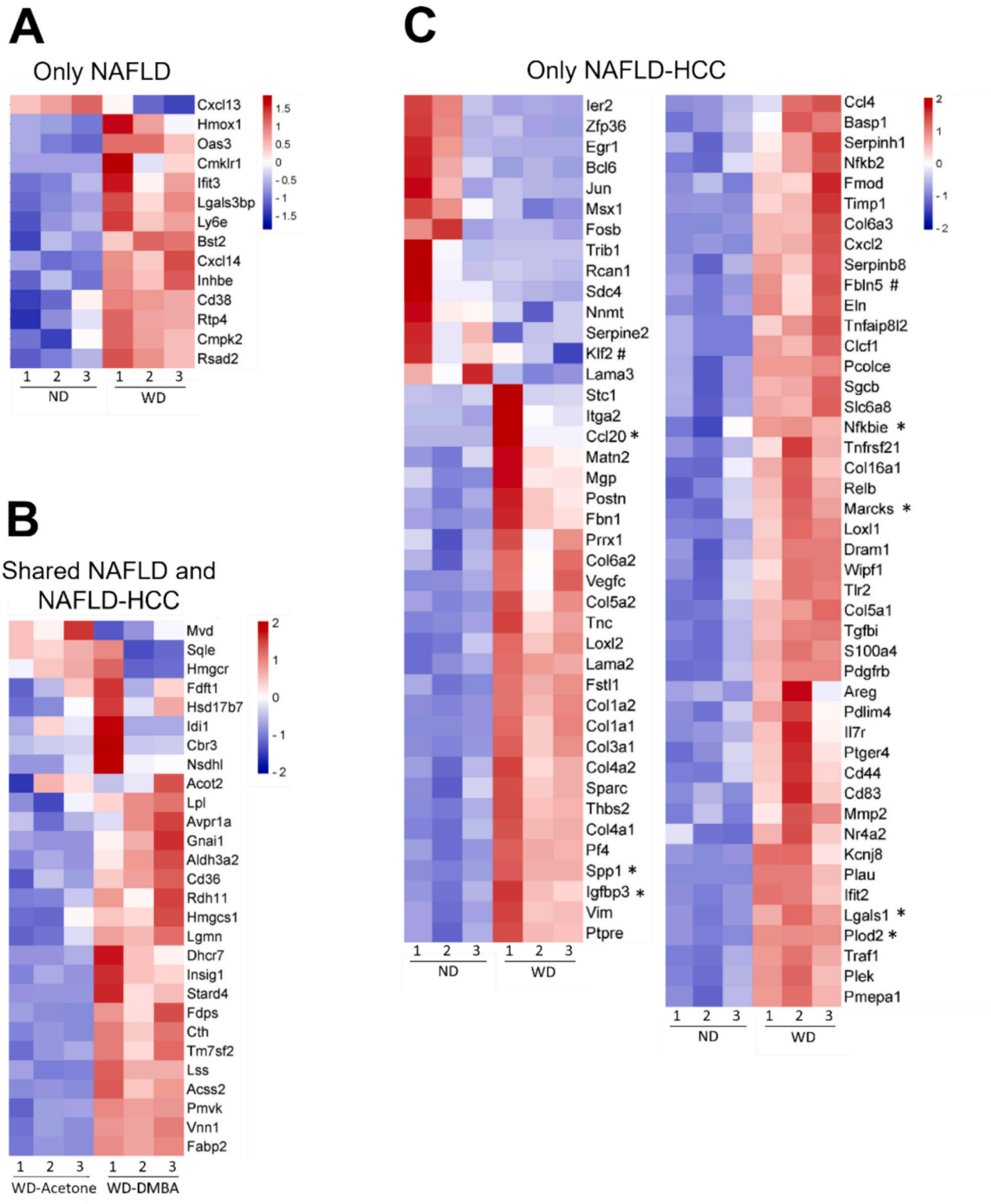


Fig. 4. Individual gene signatures of NAFLD and NAFLD-HCC, represented in heatmaps that display the differentially expressed genes (DEG) characteristic of each model. (A) DEG exclusively expressed in the NAFLD model. (B) DEG that correspond to the overlapping genes between the NAFLD and NAFLD-HCC model. (C) DEG that are exclusively expressed in the NAFLD-HCC. # - genes with a good prognosis in HCC, * - genes with a bad prognosis in HCC (according to the Human Protein Atlas). For all analyses a false discovery rate (FDR)-adjusted p value of <0.05 and a log2-fold change >1 were used. $n = 3$ per group.

associated with cholesterol metabolism, bile acid metabolism, mammalian target of rapamycin complex 1 (mTORC1) signaling, xenobiotic metabolism, immune response, and FA metabolism (Fig. 3F).

To understand how the transcriptional signature varies in each model, a Venn diagram was used to separate DEG into three categories: (i) DEG exclusively expressed in the NAFLD model, (ii) DEG overlapping between the NAFLD and NAFLD-HCC model, and (iii) DEG exclusively expressed in the NAFLD-HCC model (Fig. 3G). Enrichment analysis and prediction of TFEA targeting the list of DEG were performed using ChEA3 [40] for each gene set. In the NAFLD model, only 221 DEG were exclusive to the model. Enrichment analysis showed that the genes were mainly related to inflammation (Fig. 3H). TFEA revealed that approximately 7 % of the genes were regulated by the early growth response protein 1 (Egr1) and 8 % by the nuclear receptor subfamily 1 group I member (NR1l2). For the overlapping gene list of the NAFLD and NAFLD-HCC model (311 DEG), enrichment analysis revealed that most of the genes were involved in FA metabolism. However, no predicted TFEA was found (Fig. 3I). In the list of genes exclusively expressed in the NAFLD-HCC group (871 DEG), characteristic signatures of carcinogenesis were enriched. Additionally, the basic helix-loop-helix transcription factor T-cell acute lymphocytic leukemia 1 (erythroid differentiation factor, Tal1) was predicted to regulate >11 % of the genes in this set (Fig. 3J).

DEG obtained from the analysis were plotted in heatmaps for their visual representation (Fig. 4). Consistent with previous analyses, the majority of DEG found in the NAFLD model were upregulated as a result of the WD (Fig. 4A). For the DEG shared between NAFLD and NAFLD-HCC, a group of genes primarily involved in cholesterol metabolism was identified, while it varies between the models (Fig. 4B). Finally, the DEG expressed only in the NAFLD-HCC model could be categorized into clusters of downregulated and upregulated genes (Fig. 4C). The downregulated genes identified are involved in the nuclear factor kappa-light-chain-enhancer of activated B cells (NF-κB) signaling pathway, while the upregulated cluster contained genes involved in EMT and angiogenesis.

Interestingly, we found that high expressions of C-C motif chemokine ligand 20 (Ccl20), secreted phosphoprotein 1 (Spp1), insulin like growth factor binding protein 3 (Igfbp3), NF-κB inhibitor epsilon (Nfkbie), myristoylated alanine-rich protein kinase C substrate (Marcks), galectin 1 (Lgals1) and procollagen-lysine-2-oxoglutarate- 5-dioxygenase 2 (Plod 2) (Fig. S1) were predicted to have an unfavorable prognosis in liver cancer according to the Human Protein Atlas (www.proteinatlas.org, last accessed 23 January 2024) [41]. These data suggest that mice affected by a carcinogenic process present higher expression of inflammation-related genes and genes associated with EMT compared to mice that only developed NAFLD.

3.3. *De novo lipogenesis, TAG and cholesterol synthesis are altered in mice fed with a Western diet*

Since we observed that several genes altered in the different diets

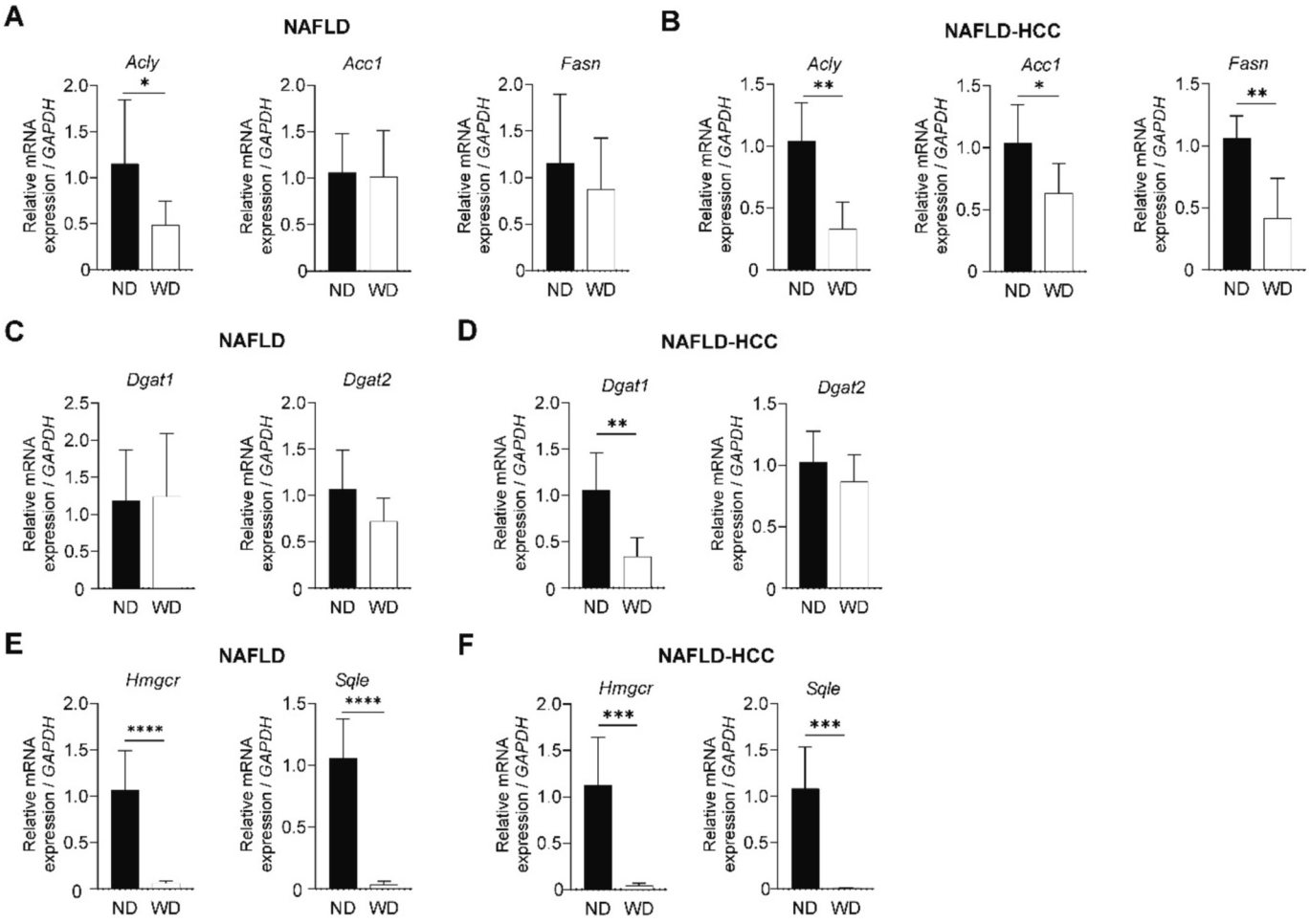


Fig. 5. Lipid homeostasis is altered differently in NAFLD and NAFLD-HCC. The expression of markers related to (A, B) *de novo* lipogenesis, (C, D) triacylglycerol synthesis, and (E, F) cholesterol synthesis was assessed using RT-qPCR in the NAFLD and NAFLD-HCC models. The study included 5–8 mice per group with two technical replicates per mouse. The data presented are the mean ± SD. For each gene *t*-tests were performed. Acly, ATP citrate lyase; Acc1, Acetyl-CoA carboxylase α; Dgat, Diacylglycerol acyltransferase; Fasn, Fatty acid synthase; Hmgcr, 3-Hydroxy-3-methylglutaryl-CoA reductase; Sqle, Squalene epoxidase. $^{*}p < 0.05$, $^{**}p < 0.01$, $^{***}p < 0.001$, $^{****}p < 0.0001$.

were related to FA and cholesterol homeostasis, we decided to evaluate the expression of genes implicated in *de novo* lipogenesis and synthesis of cholesterol. Obtained results revealed that the expression of key genes that support FA synthesis such as ATP citrate lyase (Acly) and FA synthase (Fasn) were significantly reduced in mice fed a WD compared to their ND littermates. However, this applies exclusively in the NAFLD-HCC model. In the NAFLD model, a significant decrease was observed only for Acly (Fig. 5A, B). Furthermore, we evaluated whether triacylglycerols (TAG) or cholesterol biosynthesis were impaired in mice fed with a WD. The results showed that mice challenged with the WD coordinate TAG synthesis by downregulating the expression of diacylglycerol acyltransferase-1 (Dgat1). Interestingly, this difference was only significant in the NAFLD-HCC model (Fig. 5C, E). Moreover, when we evaluated the expression of 3-hydroxy-3-methylglutaryl-CoA reductase (Hmgcr) and squalene epoxidase (Sqle), we found a significant decrease in these markers in both models, confirming the results obtained from the RNA-seq analysis (Fig. 4D, F). These data collectively indicate that a WD abolishes the expression of key markers regulating lipid biosynthesis in the liver.

3.4. Lipidomics analysis

3.4.1. The lipid composition of the food displays the liver lipid profile

While the amounts of lipids in the diets differ substantially (ND 3.3 %, WD approx. 20 % fat), the mass spectra of the dietary lipid extracts also revealed differences in the lipid composition (Fig. S2). ND mainly consisted of linoleic acid (C18:2) with small amounts of palmitic acid (C16:0), linolenic acid (C18:3), and oleic acid (C18:1). On the other hand, HFD was composed of C16:0, stearic acid (C18:0), oleic acid (C18:1) and C18:2. Additionally, ND contained lecithin, especially phosphatidylcholine (PC) 36:4, probably PC 18:2/18:2. Due to its high double bond content, this PC is prone to oxidation. Thus, lysophosphatidylcholines (LPC), especially LPC 18:2, and the corresponding FA C18:2 were also detectable in ND. The diets also differed in the composition of diacylglycerols (DAG) and TAG especially regarding their degree of unsaturation. ND showed higher amounts of DAG 36:4, TAG 52:4, TAG 54:6, TAG 54:5 and TAG 54:4, while HFD had more DAG 34:1, DAG 36:2, TAG 52:2 and TAG 54:3.

The lipid composition of the different diets is closely reflected in the liver lipid profile of the mice. The absolute amount of lipids, especially DAG and TAG, within the liver is significantly higher in HFD-fed animals compared to ND-fed mice (Fig. S3). However, the relative amounts of none of the three classes changed due to any treatment (Fig. S4). Furthermore, the composition of the diets is reflected particularly by the apolar lipids. While CE 18:2 is more abundant in ND livers, CE 18:1 occurs in larger amounts in HFD liver samples (Fig. 6A). This can most likely be directly attributed to the higher content of C18:2 in the ND chow. This is also reflected by the double bond contents (Fig. 6C). However, there are no gross differences in the chain length (Fig. 6B).

For DAG, the differences between liver samples from ND and HFD were most pronounced for DAG 34:2 and DAG 36:4, which were higher in ND. On the other hand, DAG 34:1 and DAG 36:2 were more

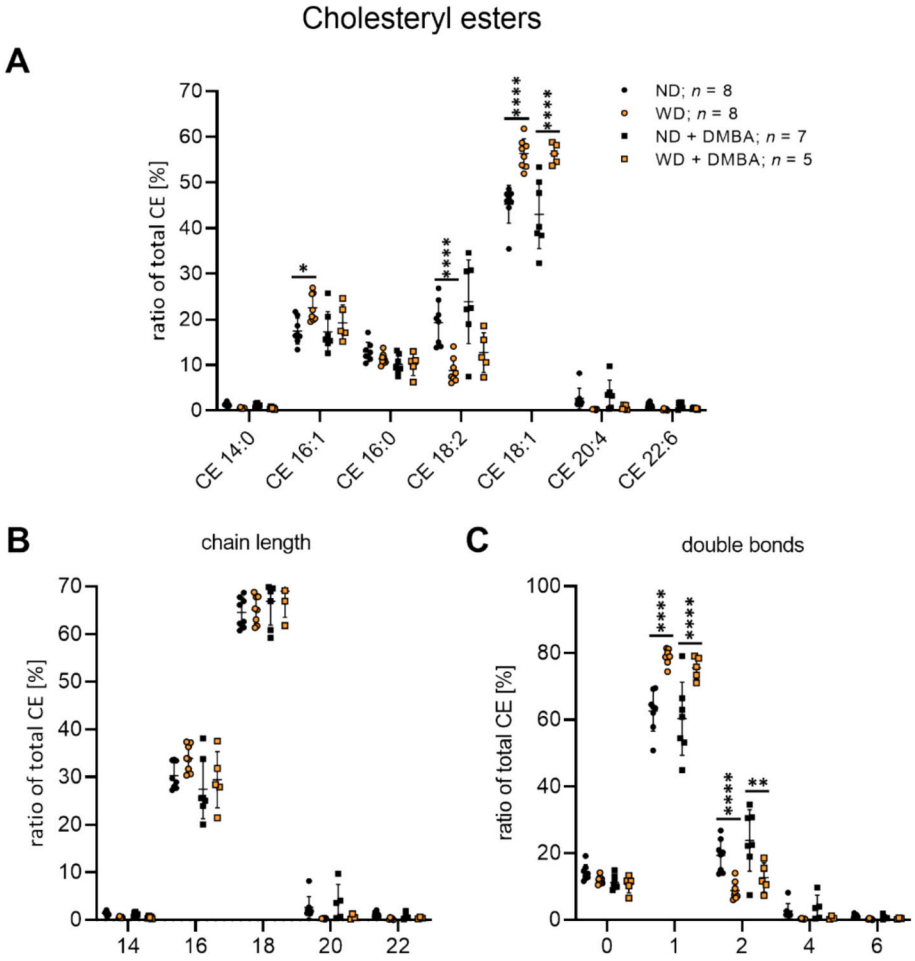


Fig. 6. Cholesteryl ester (CE) profiles of liver lipid extracts in NAFLD and NAFLD-HCC mice. The intensities of all CE species were normalized to 100 %, and the relative amounts of each CE species (A), the number of carbon atoms (B), and the number of double bonds within the fatty acyl residues (C) were calculated. The data were compared using two-way ANOVA and Tukey's multiple comparisons test. The figures show both individual values and the mean ± SD. Statistical significance is indicated as follows: *$p < 0.05$, **$p < 0.01$, ***$p < 0.001$, ****$p < 0.0001$.

pronounced in HFD (Fig. 7A). This difference is also reflected in the chain lengths of the fatty acyl residues (Fig. 7B) and the distribution of the double bond contents (Fig. 7C).

An integration of C18:1 and C18:2 from HFD is also evident in the phospholipid fractions. The relative amounts of PC 36:3 (likely composed of 18:1_18:2), PC 36:2 (presumably 18:1_18:1 and/or 18:0_18:2) and PC 38:5 (possibly 18:1_20:4 and/or 18:0_20:5 and/or 16:0_22:5) are significantly higher in HFD livers compared to ND livers (Fig. 8A). In contrast, PC 34:2 (likely 16:0_18:2) is more abundant in ND livers, which agrees with the higher amount of C18:2 in ND. The increased availability of octadecyl residues is reflected in a higher ratio of PC molecules with 36 carbon atoms in the fatty acyl chains (Fig. 8B). Depending on the diet, there is a shift from more PC molecules with 2 double bounds in the fatty acyl residues (ND) to 3 double bounds (HFD, Fig. 8C).

Phosphatidylinositol (PI) and phosphatidylethanolamine (PE), which are primarily found in the inner leaflet of biological membranes, exhibit similar patterns. In the PI molecules, there is a higher proportion of 36 carbon atoms in ND livers, as well as an increase in PI with 38 carbon atoms (Fig. 9B). Additionally, HFD liver samples showed a higher degree of unsaturation (>4 double bonds, Fig. 9C). Regarding PE, PE 38:5 and PE 40:7 (likely 18:1_22:6 and/or 18:2_22:5) are more abundant, while the contributions of PE 38:4 and PE 38:6 decreased in HFD livers compared to ND livers (Fig. S5A). Analyzing the double bonds, it is evident that PE is more unsaturated in HFD livers (with >5 double bonds, Fig. S5C) compared to ND livers (with more 4 double bonds).

For cardiolipins (CL), feeding with HFD results in a higher ratio of CL 72:6 and a lower proportion of CL 72:8 and CL 72:7 compared to ND, regardless of the presence of a NAFLD or a NAFLD-HCC phenotype (Fig. S6A and B).

In the case of sphingomyelin (SM), the observed dietary effects may not be directly attributed to the different FA compositions of the chows supplied. However, when looking at the different SM molecules, the amount of SM d18:1/16:0 is higher in mice fed a HFD compared to those provided with a ND (Fig. 10). Interestingly, SM species containing very long saturated fatty acyl chains, specifically SM d18:1/22:0 and SM d18:1/24:0 are more abundant in mice fed a ND.

Interestingly, there was no impact of DMBA on the liver lipid profile and the development of HCC. Instead, the differences in the lipid composition of the liver seem to be primarily influenced by the lipid composition of the diet. This is evident as samples from the same diets (with or without DMBA treatment) cluster closely together in principal component analysis (PCA, Fig. 11).

4. Discussion

In this study, we examined both profiles in mouse models of NAFLD and NAFLD-HCC. In the first model, mice were fed with a HFD enriched with glucose/fructose water (WD), mimicking the development of NAFLD. In the second model, mice were treated with DMBA and then fed a WD.

Histological analyses of liver sections from the NAFLD and NAFLD-HCC models revealed that mice fed a WD exhibited intrahepatic

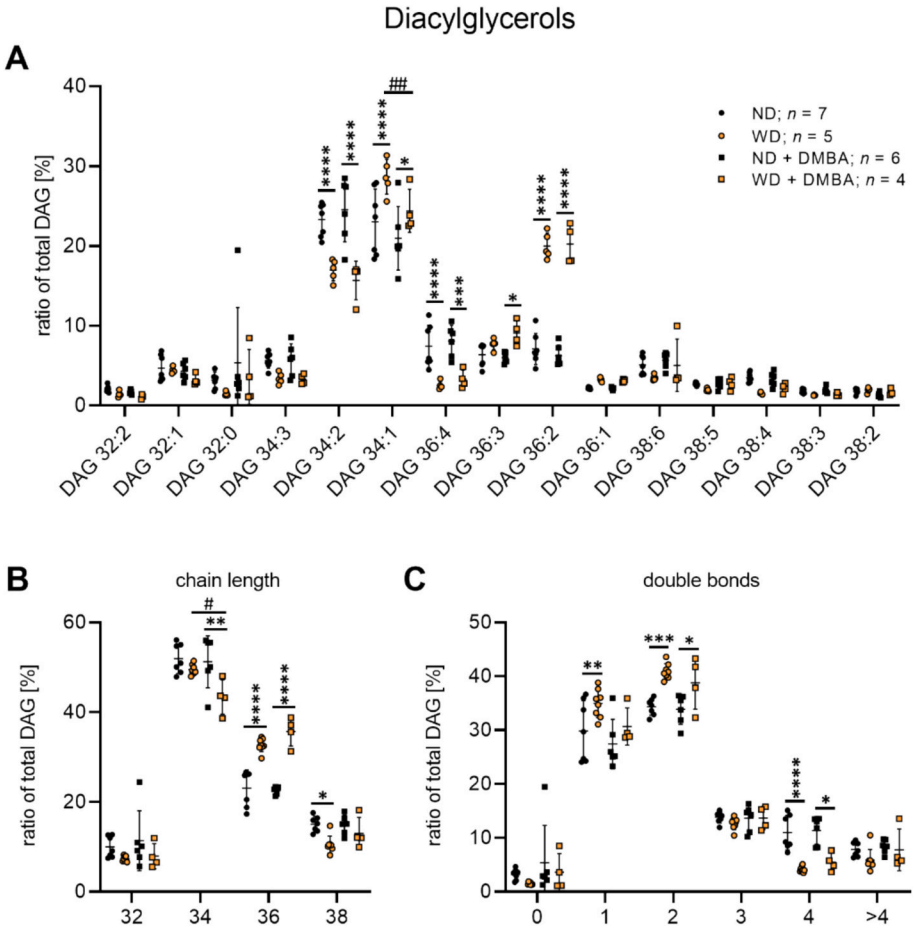


Fig. 7. Diacylglycerol (DAG) profiles of liver lipid extracts in NAFLD and NAFLD-HCC mice. The intensities of all DAG species were set to 100 %, and the percentage of individual DAG species (A), the number of carbon atoms (B), and the number of double bonds within the fatty acyl residues (C) were calculated. The data were compared using two-way ANOVA and Tukey's multiple comparisons test. The figure shows both, single values and the mean ± SD. $*/^{\#}p < 0.05$, $**/^{\#\#}p < 0.01$, $***p < 0.001$, $****p < 0.0001$.

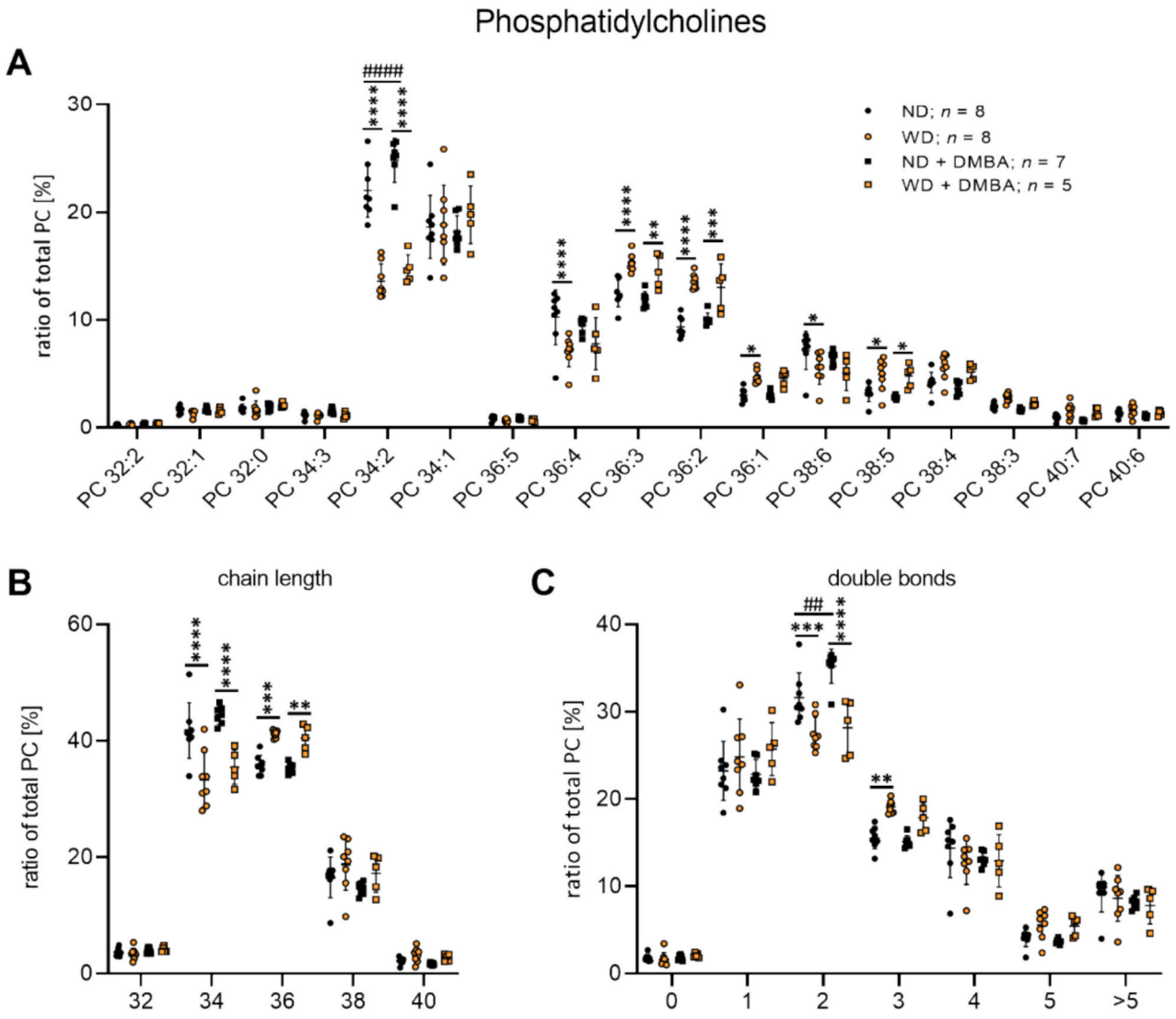


Fig. 8. Phosphatidylcholine (PC) profiles of liver lipid extracts in mice with non-alcoholic fatty liver disease (NAFLD) and NAFLD-associated hepatocellular carcinoma (NAFLD-HCC). The intensities of all PC species were normalized to 100 % and the relative contributions of each PC species (A), the number of carbon atoms (B), and the number of double bonds within the fatty acyl residues (C) were calculated. The data were analyzed using a two-way ANOVA and Tukey's multiple comparisons test. The figure includes both single values and the mean ± SD. Statistical significance is indicated as follows: $^{*}p < 0.05$, $^{**/\#\#}p < 0.01$, $^{***}p < 0.001$, $^{****/\#\#\#\#}p < 0.0001$.

accumulation of various lipids accompanied by fibrosis (Fig. 2). Although fibrosis staging was not performed, our results were indicative of early stage fibrosis according to Brunt and colleagues [42]. We speculate that the inclusion of fructose in the drinking water facilitated the induction of fibrosis, as has been previously observed in other murine NAFLD models [43]. Interestingly, mice subjected to DMBA and a HFD without the addition of sugar to their drinking water showed no hepatic fibrosis [12]. These findings suggest that the simultaneous consumption of a high fat diet and fructose/glucose leads to molecular changes that promote fibrosis development. They are supported by clinical data that observe an increased risk of NAFLD due to soft drinks in human cohorts [44]. Overall, a HFD and increased sugar intake may not be considered just concomitant risk factors but rather risk multipliers for the development and progression of NAFLD.

Besides, the results from RNA-sequencing indicate that each of the models presented a distinctive transcriptional signature. Several genes involved in lipid homeostasis and immune response were found in the NAFLD model, while increased expression of markers related to EMT and inflammation were observed in the NAFLD-HCC model (Figs. 3 and 4). NAFLD progression and malignant transformation are accompanied and mediated by immune response and inflammation [45]. For example, activated macrophages have been shown to be markers for progressive steatohepatitis [46]. Reducing immune response via checkpoint inhibitors such as Atezolizumab improves the outcome of HCC patients, highlighting the importance of the immune microenvironment in the pathophysiology of HCC [47]. EMT, on the other hand, is closely related to inflammatory processes and is crucial for tumorigenesis and metastasis of HCC, especially in liver tissue undergoing fibrotic remodeling [48,49]. Upregulated genes involved in EMT, inflammation, KRAS signaling, and angiogenesis in our murine NAFLD-HCC model, closely mirror genetic alterations in human HCC, consistent with previous comparisons [50–53].

Interestingly, the genes uniquely expressed in the NAFLD model are partly regulated by Egr1, a gene that has been previously associated with insulin resistance and cholesterol biosynthesis [54], whereas NR1l2 has been predicted to regulate xenobiotic metabolism and its expression is activated by the consumption of fructose [55]. In contrast, Tal1 was predicted to act as an upstream regulator of several genes in the NAFLD-HCC model. Tal1 is a transcription factor involved in immune response and previous studies have found that its activation deregulates the

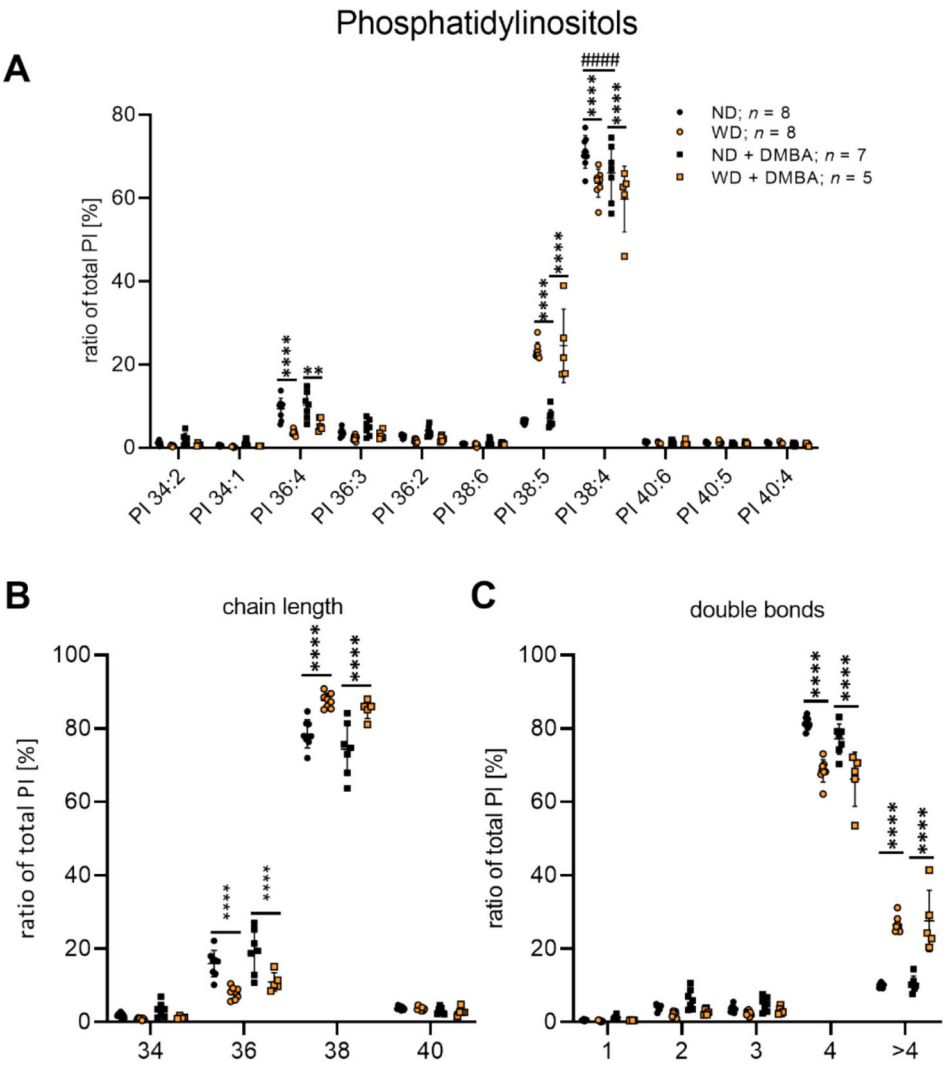


Fig. 9. Phosphatidylinositol (PI) profiles of liver lipid extracts in NAFLD and NAFLD-HCC mice. The intensities of all PI species were set to 100 % and the relative amounts of the single PI species (A), the amount of carbon atoms (B), and the amount of double bonds within the fatty acyl residues (C) were calculated. The data were compared using a two-way ANOVA and Tukey's multiple comparisons test. Single values as well as the mean ± SD are shown. $^{**}p < 0.01$, $^{****/\#\#\#\#}p < 0.0001$.

amino acid and carbohydrate metabolism leading to liver cancer development [56]. These data indicate that transcriptional reprogramming of cells influences both, the development of NAFLD and the progression of NAFLD-driven HCC. It is obvious that WD acts as a critical modulator of lipid metabolism. In the development of NAFLD, cellular functions are highly dependent on the microenvironment and the availability of FAs, which modulate membrane composition, molecular signaling, and energy supply [57]. Under normal conditions, cells prefer to use exogenous FA instead of spending energy on increasing FA synthesis [58]. Although the lipid rewiring caused by carcinogenesis is under debate, a recent study suggested that *de novo* lipogenesis is dispensable for tumor development [59]. In contrast, another study demonstrated that hepatic cancerous cells present aberrant lipid metabolism by making use of both exogenous FA and *de novo* biosynthesis [60].

Altered usage of FA may result from specific mutations within the tumor. For example, it has been reported that the mutation of oncogenic Ras leads to a preference for FA as an energy source to support growth [61]. This finding aligns with the results seen in the NAFLD-HCC model, where mice fed with a WD showed decreased expression of genes involved in *de novo* lipogenesis, but increased levels of markers involved in lipid uptake such as lipoprotein lipase (*Lpl*), cluster of differentiation 36 (*Cd36*) and FA-binding protein 2 (*Fabp2*) (Figs. 4 and 5). We speculate that aberrant lipid metabolism in the NAFLD-HCC model may be partially mediated by Ras mutations induced by DMBA. Additionally, there is evidence suggesting that lipid uptake plays a crucial role in HCC development in microenvironments enriched with FA, particularly through the overexpression of CD36, which ultimately leads to the development of an EMT phenotype and promotion of aerobic glycolysis [62,63]. On the other hand, the results obtained in the NAFLD model showed no significant changes in markers of *de novo* lipogenesis, except for *Acly*. We speculate that cells can either use circulating FA for their needs or consume sugars that increase FA synthesis [64].

When comparing the common pathway altered in both models, our results indicate that cholesterol metabolism might be significantly affected by the diet itself. Indicative changes include the reduction in the expression of *Hmgcr* and *Sqle*, which is consistent with reports showing that diets high in cholesterol inhibit its *de novo* biosynthesis [65]. These findings agree with the observed changes in the lipid composition of murine livers, which were primarily driven by the diet. For example, the fatty acyl composition of the identified apolar lipid species reflected the fatty acyl composition of the chow. Apolar lipids in ND liver samples were rich in C18:2, while apolar lipids in WD liver samples had higher levels of C18:1. There is a notable correlation between lipid accumulation and the progression of NAFLD. For instance, the presence of cholesterol crystals within hepatocyte lipid droplets has been identified

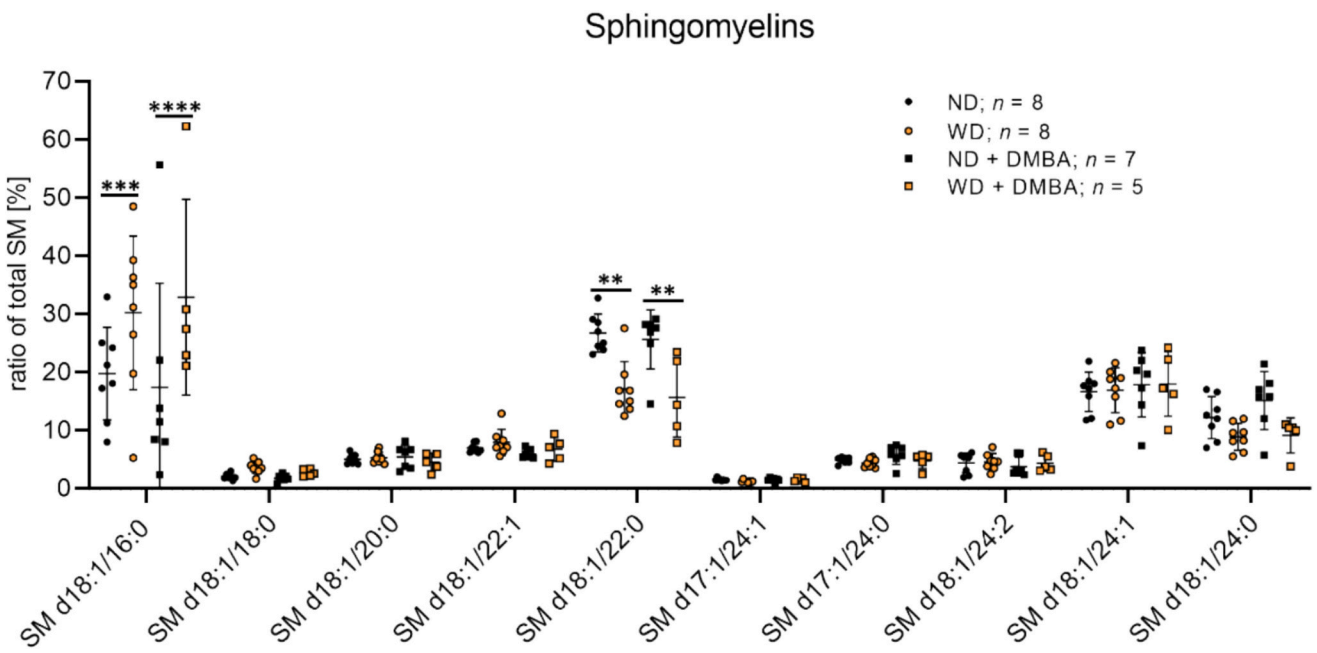


Fig. 10. Sphingomyelin (SM) profiles of liver lipid extracts in NAFLD and NAFLD-HCC mice. The intensities of all SM species were standardized to 100 % and the relative amounts of each SM species were calculated. The percentages of relative amounts of SM species are presented. The data were compared using a two-way ANOVA and Tukey's multiple comparisons test. Both individual values and the mean ± SD are displayed. $^{**}p < 0.01$, $^{***}p < 0.001$, $^{****}p < 0.0001$.

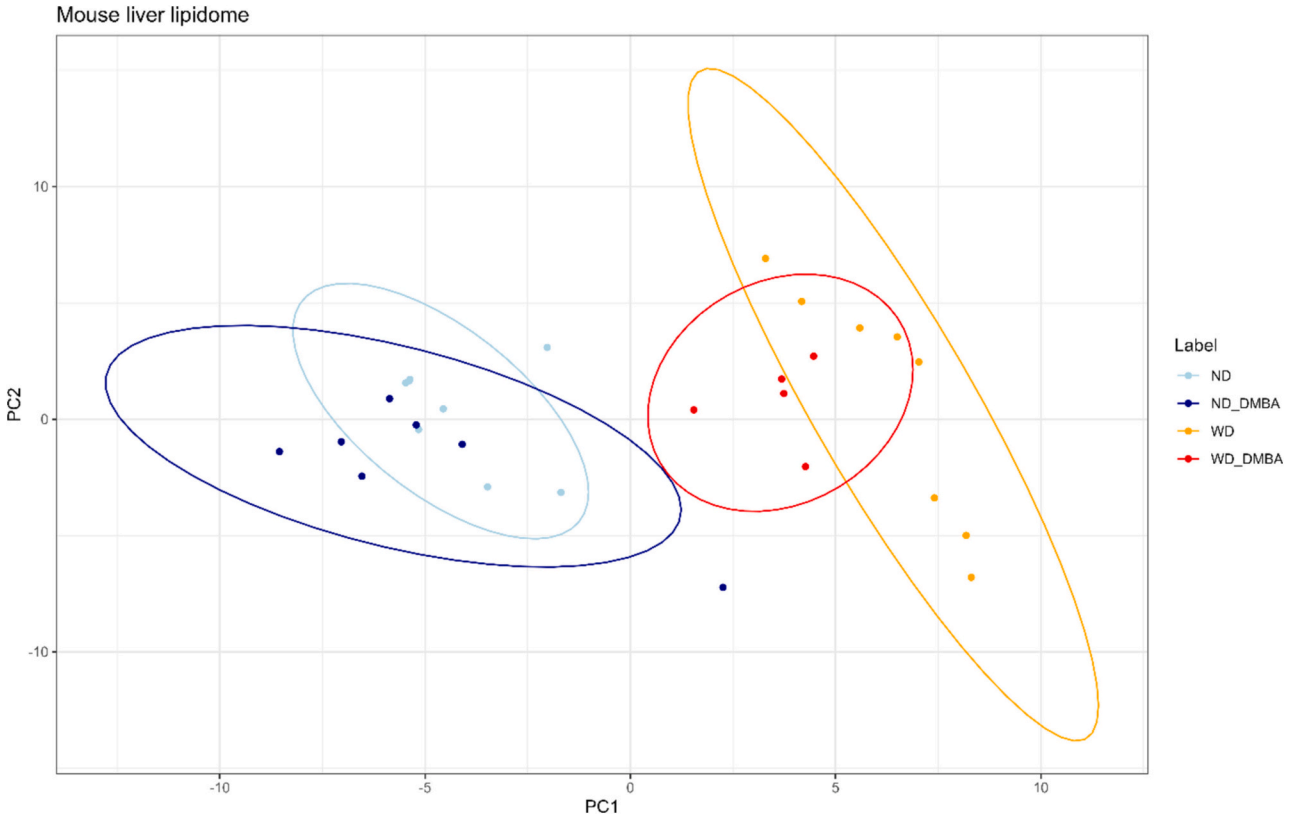


Fig. 11. Principal component analysis (PCA) of all detected lipids. The variables were scaled to have unit variance. The color-coding scheme according to group labels is depicted in the legend on the right margin.

as a marker for fibrosing NASH, which is primarily driven by dietary factors [66]. These findings suggest that diet plays a significant role in the pathophysiology of NAFLD.

Accumulation of DAG within the liver is considered a key event in the development of NAFLD, a phenomenon known as 'lipotoxicity' [67]. It has been reported that this effect is largely attributable to the diet, which is consistent with our results. For instance, hepatic DAG overload has been shown to activate protein kinase C (PKC)-ε, impairing insulin

receptor activation and glycogen synthesis [68]. PKC activation is also considered an important mediator in carcinogenesis [69]. Although overall DAG concentrations did not differ between the groups, we observed a different composition of DAG in liver samples of mice fed a WD. Monounsaturated DAG 34:1 and mono- or di-unsaturated 36:2 significantly increased at the expense of polyunsaturated species, which is consistent with previous findings [70]. DAG subspecies-specific activation of PKC has been reported previously [71], suggesting that diet-induced changes in DAG composition may play a crucial role in cancer development. Our results also demonstrated a suppression of *Dgat1* exclusively in the NAFLD-HCC model. Dgat1 has been shown to be more susceptible to monounsaturated acyl chains and more potent under conditions with high substrate concentrations [72]. Additionally, *Dgat1*-deficient murine fibroblasts were found to be susceptible to cell death when treated with oleate, suggesting protective effects of *Dgat1* against lipotoxicity [73]. However, lipid analysis did not reveal any significant change in the amount of DAG after DMBA treatment.

Other lipidomic changes may be more indicative of the progression of the disease, as they are not directly linked to the lipid composition of the diet, but rather to subsequent changes in the liver. Interestingly, the treatment with DMBA did not appear to have any effect on the observed lipid compositions. However, changes in the diet had a much more significant effect on the fatty acyl compositions of all lipid classes. This finding aligns with a study by Rao and colleagues, who discovered that the lipid composition of the diet and the duration of the feeding experiment, in addition to DMBA treatment, affect the lipid composition of rat organs [74].

In this study, lipid analysis revealed an increase in the ratio of SM d18:1/16:0 and a decrease in SM species containing very long fatty acyl chains (C22:0 and C24:0) in mice on the WD. Changes in the sphingolipid profile are often discussed as potential contributors to the development of NAFLD [75]. Previous lipidomic analysis of human liver biopsies has also shown significant changes in the levels of certain SM species, which could serve as markers for the progression of NAFLD [76]. Decreased concentrations of the very long fatty acyl chain-containing lipids SM d40:1 and SM d42:1 have been closely associated with the progression of NAFLD in mice liver [77], as well as with hepatic injury and elevated inflammation levels in patients with chronic hepatitis B, respectively [78].

CLs are believed to be exceptionally vulnerable to oxidative stress due to their positioning on the inner mitochondrial membrane and, consequently, their exposure to reactive oxygen species [79]. Their profile shows significant changes in human NAFLD- and NASH-liver samples. In particular, an increase in monounsaturated acyl chains and a decrease in di-unsaturated acyl chains were reported [80,81]. These results were evident in rats subjected to a HFD [82]. We also demonstrated a marked shift in the distribution of CL in our NAFLD- and NAFLD-HCC models, respectively. In both models, the cumulative number of double bonds in different CL specimens significantly decreased. Such changes are believed to reflect a “rescue attempt” in the face of accumulating liver damage [79].

We also observed a higher content of unsaturated PC, PE and PI in mice fed with a WD. Similar results for individual specimens of these groups have been reported for both human cirrhotic and murine steatotic liver samples, respectively, in which changes in the DAG composition were exclusively discussed [70].

Due to the absence of effects of DMBA on lipid levels, we assume that the observed changes at the genomic level are compensated by the organism to some extent in order to safeguard proper functionality as much as possible.

5. Conclusions

In summary, the NAFLD-HCC model used in our study accurately mimics human NAFLD-induced HCC, which has a poor prognosis. We discovered that crucial cellular processes for carcinogenesis are greatly enhanced in DMBA-treated mice that are also subjected to WD. Additionally, our study shows that combining HFD with glucose/fructose promotes the development of liver tumors. There are notable differences in the progression of NAFLD and NAFLD-HCC, which can be seen in gene expression changes affecting hepatic inflammatory response and FA metabolism. Analysis of lipid profiles revealed that the diet has a significant impact on lipid composition, emphasizing the important role of nutrition in hepatic lipotoxicity and carcinogenesis.

Supplementary data to this article can be found online at https://doi.org/10.1016/j.bbalip.2024.159574.

CRediT authorship contribution statement

Marvin Leopold: Writing – review & editing, Writing – original draft, Visualization, Validation, Methodology, Investigation, Formal analysis, Data curation. **Paola Berenice Mass-Sanchez:** Writing – review & editing, Writing – original draft, Visualization, Validation, Methodology, Investigation, Formal analysis, Data curation. **Marinela Krizanac:** Writing – review & editing, Methodology. **Paula Štancl:** Writing – review & editing, Methodology. **Rosa Karlić:** Writing – review & editing, Methodology. **Patricia Prabutzki:** Writing – review & editing, Visualization, Methodology, Data curation. **Victoria Parafianczuk:** Methodology, Data curation. **Jürgen Schiller:** Resources, Funding acquisition. **Anastasia Asimakopoulos:** Writing – review & editing, Supervision, Project administration, Funding acquisition, Conceptualization. **Kathrin M. Engel:** Writing – review & editing, Visualization, Supervision, Resources, Methodology, Funding acquisition, Conceptualization. **Ralf Weiskirchen:** Writing – review & editing, Supervision, Resources, Project administration, Funding acquisition, Conceptualization.

Institutional review board statement

The animal study protocol was approved by the institutional German Animal Care Committee (LANUV, Recklinghausen, Germany, permit Az.: 81-02.04.2019.A366).

Funding

A.A. received funding from the Wilhelm Sander Stiftung (project 2020.002.1) and the START program (project 102/20). R.W. is supported by the German Research Foundation (grants WE2554/13-1, WE2554/15-1, and WE 2554/17-1), a grant from the Interdisciplinary Centre for Clinical Research within the Faculty of Medicine at the RWTH Aachen University (IZKF, PTD 1-5), and a grant from the Deutsche Krebshilfe (project 70115581). K.M.E. and J.S. are supported by the German Research Foundation (EN 1279/3-1 to K.M.E.; SCHI 476/19-1 and SFB 1052, project Z3 to J.S.). P.Š. and R.K. were funded by grants from the Croatian National Science Foundation Project PREDI-COO (project IP-2019-04-9308).

Declaration of competing interest

The authors declare that they have no known competing financial interests or personal relationships that could have appeared to influence the work reported in this paper.

Data availability

The data that support the findings of this study are available from the corresponding authors upon reasonable request. The RNA-seq data that support the findings of this study were submitted to the Gene Expression Omnibus (GEO, https://www.ncbi.nlm.nih.gov/geo/) under access. no. GSE242852.

References

[1] M.H. Le, Y.H. Yeo, X. Li, J. Li, B. Zou, Y. Wu, Q. Ye, D.Q. Huang, C. Zhao, J. Zhang, C. Liu, N. Chang, F. Xing, S. Yan, Z.H. Wan, N.S.Y. Tang, M. Mayumi, X. Liu, C. Liu, F. Rui, H. Yang, Y. Yang, R. Jin, R.H.X. Le, Y. Xu, D.M. Le, S. Barnett, C.D. Stave, R. Cheung, Q. Zhu, M.H. Nguyen, Global NAFLD prevalence: a systematic review and meta-analysis, Gastroenterol. Hepatol. 20 (2019) 2809–2817, e28, https://doi.org/10.1016/j.cgh.2021.12.002.

[2] K. Riazi, H. Azhari, J.H. Charette, F.E. Underwood, J.A. King, E.E. Afshar, M. G. Swain, S.E. Congly, G.G. Kaplan, A.A. Shaheen, The prevalence and incidence of NAFLD worldwide: a systematic review and meta-analysis, Lancet Gastroenterol. Hepatol. 7 (2022) 851–861, https://doi.org/10.1016/S2468-1253(22)00165-0.

[3] C. Estes, H. Razavi, R. Loomba, Z. Younossi, A.J. Sanyal, Modeling the epidemic of nonalcoholic fatty liver disease demonstrates an exponential increase in burden of disease, Hepatology 67 (2018) 123–133, https://doi.org/10.1002/hep.29466.

[4] A. Mantovani, G. Petracca, G. Beatrice, A. Csermely, H. Tilg, C.D. Byrne, G. Targher, Non-alcoholic fatty liver disease and increased risk of incident extrahepatic cancers: a meta-analysis of observational cohort studies, Gut 71 (2022) 778–788, https://doi.org/10.1136/gutjnl-2021-324191.

[5] M. Eslam, A.J. Sanyal, J. George, International Consensus Panel, MAFLD: a consensus-driven proposed nomenclature for metabolic associated fatty liver disease, Gastroenterology 158 (2020) 1999–2014.e1, https://doi.org/10.1053/j.gastro.2019.11.312.

[6] B. Paul, M. Lewinska, J.B. Andersen, Lipid alterations in chronic liver disease and liver cancer, JHEP Rep. 4 (2022) 100479, https://doi.org/10.1016/j.jhepr.2022.100479.

[7] H. Tilg, T.E. Adolph, A.R. Moschen, Multiple parallel hits hypothesis in nonalcoholic fatty liver disease: revisited after a decade, Hepatology 73 (2021) 833–842, https://doi.org/10.1002/hep.31518.

[8] E. Buzzetti, M. Pinzani, E.A. Tsochatzis, The multiple-hit pathogenesis of non-alcoholic fatty liver disease (NAFLD), Metabolism 65 (2016) 1038–1048, https://doi.org/10.1016/j.metabol.2015.12.012.

[9] D.Q. Huang, H.B. El-Serag, R. Loomba, Global epidemiology of NAFLD-related HCC: trends, predictions, risk factors and prevention, Nat. Rev. Gastroenterol. Hepatol. 18 (2021) 223–238, https://doi.org/10.1038/s41575-020-00381-6.

[10] M.A. Febbraio, S. Reibe, S. Shalapour, G.J. Ooi, M.J. Watt, M. Karin, Preclinical models for studying NASH-driven HCC: how useful are they? Cell Metab. 29 (2019) 18–26, https://doi.org/10.1016/j.cmet.2018.10.012.

[11] Y.R. Im, H. Hunter, D. de Gracia Hahn, A. Duret, Q. Cheah, J. Dong, M. Fairey, C. Hjalmarsson, A. Li, H.K. Lim, L. McKeown, C.G. Mitrofan, R. Rao, M. Utukuri, I. A. Rowe, J.P.A. Mann, Systematic review of animal models of NAFLD finds high-fat, high-fructose diets most closely resemble human NAFLD, Hepatology 74 (2021) 1884–1901, https://doi.org/10.1002/hep.31897.

[12] S. Yoshimoto, T.M. Loo, K. Atarashi, H. Kanda, S. Sato, S. Oyadomari, Y. Iwakura, K. Oshima, H. Morita, M. Hattori, K. Honda, Y. Ishikawa, E. Hara, N. Ohtani, Obesity-induced gut microbial metabolite promotes liver cancer through senescence secretome, Nature 499 (2013) 97–101, https://doi.org/10.1038/nature12347.

[13] Y. Niwa, K. Ishikawa, M. Ishigami, T. Honda, K. Achiwa, T. Izumoto, R. Maekawa, K. Hosokawa, A. Iida, Y. Seino, Y. Hamada, H. Goto, Y. Oiso, H. Arima, S. Tsunekawa, Effect of hyperglycemia on hepatocellular carcinoma development in diabetes, Biochem. Biophys. Res. Commun. 463 (2015) 344–350, https://doi.org/10.1016/j.bbrc.2015.05.066.

[14] A. Kroh, J. Walter, H. Schüler, J. Nolting, R. Eickhoff, D. Heise, U.P. Neumann, T. Cramer, T.F. Ulmer, A. Fragoulis, A newly established murine cell line as a model for hepatocellular cancer in non-alcoholic steatohepatitis, Int. J. Mol. Sci. 20 (2019) 5658, https://doi.org/10.3390/ijms20225658.

[15] S.A. Gurses, S. Banskar, C. Stewart, B. Trimoski, R. Dziarski, D. Gupta, Nod2 protects mice from inflammation and obesity-dependent liver cancer, Sci. Rep. 10 (2020) 20519, https://doi.org/10.1038/s41598-020-77463-7.

[16] M. Jamalinia, A. Lonardo, R. Weiskirchen, Sex and gender differences in liver fibrosis: Pathomechanisms and clinical outcomes, Fibrosis 2 (2024) 10006, https://doi.org/10.70322/fibrosis.2024.10006.

[17] A. Asimakopoulou, K.M. Engel, N. Gassler, T. Bracht, B. Sitek, E.M. Buhl, S. Kalampoka, M. Pinoé-Schmidt, J. van Helden, J. Schiller, R. Weiskirchen, Deletion of Perilipin 5 protects against hepatic injury in nonalcoholic fatty liver disease via missing inflammasome activation, Cells 9 (2020) 1346, https://doi.org/10.3390/cells9061346.

[18] J.R.C. Nunes, T.K.T. Smith, P. Ghorbani, C. O'Dwyer, N.A. Trzaskalski, H. Dergham, C. Pember, M.K. Kilgour, E.E. Mulvihill, M.D. Fullerton, Thermoneutral housing does not accelerate metabolic dysfunction-associated fatty liver disease in male or female C57Bl/6J mice fed a Western diet, Am. J. Physiol. Endocrinol. Metab. 325 (2023) E10–E20, https://doi.org/10.1152/ajpendo.00124.2023.

[19] D.A. Giles, M.E. Moreno-Fernandez, T.E. Stankiewicz, S. Graspeuntner, M. Cappelletti, D. Wu, R. Mukherjee, C.C. Chan, M.J. Lawson, J. Klarquist, A. Sünderhauf, S. Softic, C.R. Kahn, K. Stemmer, Y. Iwakura, B.J. Aronow, R. Karns, K.A. Steinbrecher, C.L. Karp, R. Sheridan, S.K. Shanmukhappa, D. Reynaud, D. B. Haslam, C. Sina, J. Rupp, S.P. Hogan, S. Divanovic, Thermoneutral housing exacerbates nonalcoholic fatty liver disease in mice and allows for sex-independent disease modeling, Nat. Med. 23 (2017) 829–838, https://doi.org/10.1038/nm.4346 (Erratum in: Nat Med. 2017, 23, 1241. doi:10.1038/nm1017-1241c).

[20] K.J. Livak, T.D. Schmittgen, Analysis of relative gene expression data using real-time quantitative PCR and the 2(-Delta Delta C(T)) Method, Methods (San Diego, Calif.) 25 (2001) 402–408, https://doi.org/10.1006/meth.2001.1262.

[21] E. Borkham-Kamphorst, U. Haas, M. Pinoé-Schmidt, A.T. Abdallah, R. Weiskirchen, Chronic mineral oil administration increases hepatic inflammation in wild type mice compared to lipocalin 2 null mice, Lab. Investig. 101 (2021) 1528–1539, https://doi.org/10.1038/s41374-021-00672-9.

[22] A. Dobin, C.A. Davis, F. Schlesinger, J. Drenkow, C. Zaleski, S. Jha, P. Batut, M. Chaisson, T.R. Gingeras, STAR: ultrafast universal RNA-seq aligner, Bioinformatics 29 (2013) 15–21, https://doi.org/10.1093/bioinformatics/bts635.

[23] Y. Liao, G.K. Smyth, W. Shi, featureCounts: an efficient general purpose program for assigning sequence reads to genomic features, Bioinformatics 30 (2014) 923–930, https://doi.org/10.1093/bioinformatics/btt656.

[24] K. Raivo, pheatmap: pretty heatmaps, R package version 1.0.12, https://CRAN.R-project.org/package=pheatmap, 2019.

[25] M.I. Love, W. Huber, S. Anders, Moderated estimation of fold change and dispersion for RNA-seq data with DESeq2, Genome Biol. 15 (2014) 550, https://doi.org/10.1186/s13059-014-0550-8.

[26] A. Zhu, J.G. Ibrahim, M.I. Love, Heavy-tailed prior distributions for sequence count data: removing the noise and preserving large differences, Bioinformatics 35 (2019) 2084–2092, https://doi.org/10.1093/bioinformatics/bty895.

[27] S.X. Ge, D. Jung, R. Yao, ShinyGO: a graphical gene-set enrichment tool for animals and plants, Bioinformatics 36 (2020) 2628–2629, https://doi.org/10.1093/bioinformatics/btz931.

[28] E.Y. Chen, C.M. Tan, Y. Kou, Q. Duan, Z. Wang, G.V. Meirelles, N.R. Clark, A. Ma'ayan, Enrichr: interactive and collaborative HTML5 gene list enrichment analysis tool, BMC Bioinformatics 14 (2013) 128, https://doi.org/10.1186/1471-2105-14-128.

[29] M.V. Kuleshov, M.R. Jones, A.D. Rouillard, N.F. Fernandez, Q. Duan, Z. Wang, S. Koplev, S.L. Jenkins, K.M. Jagodnik, A. Lachmann, M.G. McDermott, C. D. Monteiro, G.W. Gundersen, A. Ma'ayan, Enrichr: a comprehensive gene set enrichment analysis web server 2016 update, Nucleic Acids Res. 44 (2016) W90–W97, https://doi.org/10.1093/nar/gkw377.

[30] Z. Xie, A. Bailey, M.V. Kuleshov, D.J.B. Clarke, J.E. Evangelista, S.L. Jenkins, A. Lachmann, M.L. Wojciechowicz, E. Kropiwnicki, K.M. Jagodnik, M. Jeon, A. Ma'ayan, Gene set knowledge discovery with Enrichr, Curr. Protoc. 1 (2021) e90, https://doi.org/10.1002/cpz1.90.

[31] A. Subramanian, P. Tamayo, V.K. Mootha, S. Mukherjee, B.L. Ebert, M.A. Gillette, A. Paulovich, S.L. Pomeroy, T.R. Golub, E.S. Lander, J.P. Mesirov, Gene set enrichment analysis: a knowledge-based approach for interpreting genome-wide expression profiles, Proc. Natl. Acad. Sci. USA 102 (2005) 15545–15550, https://doi.org/10.1073/pnas.0506580102.

[32] A. Liberzon, C. Birger, H. Thorvaldsdóttir, M. Ghandi, J.P. Mesirov, P. Tamayo, The molecular signatures database (MSigDB) hallmark gene set collection, Cell Syst. 1 (2015) 417–425, https://doi.org/10.1016/j.cels.2015.12.004.

[33] Welcome to SRplot, Available at: http://www.bioinformatics.com.cn/srplot. (Accessed 21 December 2023).

[34] E.G. Bligh, W.J. Dyer, A rapid method of total lipid extraction and purification, Can. J. Biochem. Physiol. 37 (1959) 911–917, https://doi.org/10.1139/o59-099.

[35] The R project for statistical computing, Available at: https://www.R-project.org/. (Accessed 21 December 2023).

[36] H. Wickham, M. Averick, J. Bryan, W. Chang, L.D. McGowan, R. François, G. Grolemund, A. Hayes, L. Henry, J. Hester, M. Kuhn, T.L. Pedersen, E. Miller, S. M. Bache, K. Müller, J. Ooms, D. Robinson, D.P. Seidel, V. Spinu, K. Takahashi, D. Vaughan, C. Wilke, K. Woo, H. Yutani, Welcome to the tidyverse, J. Open Source Softw. 4 (2019) 1686, https://doi.org/10.21105/joss.01686.

[37] H. Wickham, ggplot2: Elegant Graphics for Data Analysis, Springer-Verlag, New York, 2016 (ISBN 978-3-319-24277-4).

[38] Y. Yang, D.L. Smith Jr., K.D. Keating, D.B. Allison, T.R. Nagy, Variations in body weight, food intake and body composition after long-term high-fat diet feeding in C57BL/6J mice, Obesity 22 (2014) 2147–2155, https://doi.org/10.1002/oby.20811.

[39] B.R. Maharjan, S.V. McLennan, C. Yee, S.M. Twigg, P.F. Williams, The effect of a sustained high-fat diet on the metabolism of white and brown adipose tissue and its impact on insulin resistance: a selected time point cross-sectional study, Int. J. Mol. Sci. 22 (2021) 13639, https://doi.org/10.3390/ijms222413639.

[40] A.B. Keenan, D. Torre, A. Lachmann, A.K. Leong, M.L. Wojciechowicz, V. Utti, K. M. Jagodnik, E. Kropiwnicki, Z. Wang, A. Ma'ayan, ChEA3: transcription factor enrichment analysis by orthogonal omics integration, Nucleic Acids Res. 47 (2019) W212–W224, https://doi.org/10.1093/nar/gkz446.

[41] P.J. Thul, C. Lindskog, The human protein atlas: a spatial map of the human proteome, Protein Sci. 27 (2018) 233–244, https://doi.org/10.1002/pro.3307.

[42] E.M. Brunt, C.G. Janney, A.M. Di Bisceglie, B.A. Neuschwander-Tetri, B.R. Bacon, Nonalcoholic steatohepatitis: a proposal for grading and staging the histological lesions, Am. J. Gastroenterol. 94 (1999) 2467–2474, https://doi.org/10.1111/j.1572-0241.1999.01377.x.

[43] X.J. Liu, N.N. Duan, C. Liu, C. Niu, X.P. Liu, J. Wu, Characterization of a murine nonalcoholic steatohepatitis model induced by high fat high calorie diet plus fructose and glucose in drinking water, Lab. Investig. 98 (2018) 1184–1199, https://doi.org/10.1038/s41374-018-0074-z.

[44] J. Zheng, L. Zhao, J. Dong, H. Chen, D. Li, X. Zhang, M.M. Hassan, S.E. Steck, X. Li, Y.B. Xiang, H. Wang, The role of dietary factors in nonalcoholic fatty liver disease to hepatocellular carcinoma progression: a systematic review, Clin. Nutr. 41 (2022) 2295–2307, https://doi.org/10.1016/j.clnu.2022.08.018.

[45] M. Peiseler, R. Schwabe, J. Hampe, P. Kubes, M. Heikenwälder, F. Tacke, Immune mechanisms linking metabolic injury to inflammation and fibrosis in fatty liver disease - novel insights into cellular communication circuits, J. Hepatol. 77 (2022) 1136–1160, https://doi.org/10.1016/j.jhep.2022.06.012.

[46] A. Guillot, M. Winkler, M. Silva Afonso, A. Aggarwal, D. Lopez, H. Berger, M. S. Kohlhepp, H. Liu, B. Özdirik, J. Eschrich, J. Ma, M. Peiseler, F. Heymann, S. Pendem, S. Mahadevan, B. Gao, L. Diehl, R. Gupta, F. Tacke, Mapping the hepatic immune landscape identifies monocytic macrophages as key drivers of steatohepatitis and cholangiopathy progression, Hepatology 78 (2023) 150–166, https://doi.org/10.1097/HEP.0000000000000270.

[47] J.M. Llovet, F. Castet, M. Heikenwalder, M.K. Maini, V. Mazzaferro, D.J. Pinato, E. Pikarsky, A.X. Zhu, R.S. Finn, Immunotherapies for hepatocellular carcinoma, Nat. Rev. Clin. Oncol. 19 (2022) 151–172, https://doi.org/10.1038/s41571-021-00573-2.

[48] B. Sengez, B.I. Carr, H. Alotaibi, EMT and inflammation: crossroads in HCC, J. Gastrointest. Cancer 54 (2023) 204–212, https://doi.org/10.1007/s12029-021-00801-z.

[49] J. Jou, A.M. Diehl, Epithelial-mesenchymal transitions and hepatocarcinogenesis, J. Clin. Invest. 120 (2010) 1031–1034, https://doi.org/10.1172/JCI42615.

[50] L. Yu, N. Shen, Y. Shi, X. Shi, X. Fu, S. Li, B. Zhu, W. Yu, Y. Zhang, Characterization of cancer-related fibroblasts (CAF) in hepatocellular carcinoma and construction of CAF-based risk signature based on single-cell RNA-seq and bulk RNA-seq data, Front. Immunol. 13 (2022) 1009789, https://doi.org/10.3389/fimmu.2022.1009789.

[51] R. Pinyol, S. Torrecilla, H. Wang, C. Montironi, M. Piqué-Gili, M. Torres-Martin, L. Wei-Qiang, C.E. Willoughby, P. Ramadori, C. Andreu-Oller, P. Taik, Y.A. Lee, A. Moeini, J. Peix, S. Faure-Dupuy, T. Riedl, S. Schuehle, C.P. Oliveira, V.A. Alves, P. Boffetta, A. Lachenmayer, S. Roessler, B. Minguez, P. Schirmacher, J.F. Dufour, S.N. Thung, H.L. Reeves, F.J. Carrilho, C. Chang, A.V. Uzilov, M. Heikenwalder, A. Sanyal, S.L. Friedman, D. Sia, J.M. Llovet, Molecular characterisation of hepatocellular carcinoma in patients with non-alcoholic steatohepatitis, J. Hepatol. 75 (2021) 865–878, https://doi.org/10.1016/j.jhep.2021.04.049 (Erratum in: J Hepatol. 2021, 75, 1515. doi:10.1016/j.jhep.2021.09.014).

[52] J. Liu, Z. Wu, D. Han, C. Wei, Y. Liang, T. Jiang, L. Chen, M. Sha, Y. Cao, F. Huang, X. Geng, J. Yu, Y. Shen, H. Wang, L. Feng, D. Wang, S. Fang, S. Wang, Y. Shen, Mesencephalic astrocyte-derived neurotrophic factor inhibits liver cancer through small ubiquitin-related modifier (SUMO)ylation-related suppression of NF-κB/Snail signaling pathway and epithelial-mesenchymal transition, Hepatology 71 (2020) 1262–1278, https://doi.org/10.1002/hep.30917.

[53] Y.D. Luo, X.Y. Liu, L. Fang, H.Q. Yu, Y.J. Zhang, M. Chen, L.D. Zhang, C.M. Xie, Mutant Kras and mTOR crosstalk drives hepatocellular carcinoma development via PEG3/STAT3/BEX2 signaling, Theranostics 12 (2022) 7903–7919, https://doi.org/10.7150/thno.76873.

[54] N. Magee, Y. Zhang, Role of early growth response 1 in liver metabolism and liver cancer, Hepatoma Res. 3 (2017) 268–277, https://doi.org/10.20517/2394-5079.2017.36.

[55] J.H. Pan, J. Tang, K.E. Beane, M.C. Redding, Y.J. Cho, Y.J. Kim, J. Zhao, E.C. Shin, J.H. Lee, B.C. Kong, J.K. Kim, Hepatic transcriptomics analysis reveals that fructose intervention down-regulated xenobiotics-metabolising enzymes through aryl hydrocarbon receptor signalling suppression in C57BL/6N mice, Br. J. Nutr. 122 (2019) 769–779, https://doi.org/10.1017/S0007114519001612.

[56] R.C. Zou, S.F. Xiao, Z.T. Shi, Y. Ke, H.R. Tang, T.G. Wu, Z.T. Guo, F. Ni, W.X. Li, L. Wang, Identification of metabolism-associated pathways and genes involved in male and female liver cancer patients, J. Theor. Biol. 480 (2019) 218–228, https://doi.org/10.1016/j.jtbi.2019.08.011.

[57] C.C.C.R. de Carvalho, M.J. Caramujo, The various roles of fatty acids, Molecules 23 (2018) 2583, https://doi.org/10.3390/molecules23102583.

[58] E. Currie, A. Schulze, R. Zechner, T.C. Walther, R.V. Farese Jr., Cellular fatty acid metabolism and cancer, Cell Metab. 18 (2013) 153–161, https://doi.org/10.1016/j.cmet.2013.05.017.

[59] M.E. Nelson, S. Lahiri, J.D. Chow, F.L. Byrne, S.R. Hargett, D.S. Breen, E. M. Olzomer, L.E. Wu, G.J. Cooney, N. Turner, D.E. James, J.K. Slack-Davis, C. Lackner, S.H. Caldwell, K.L. Hoehn, Inhibition of hepatic lipogenesis enhances liver tumorigenesis by increasing antioxidant defence and promoting cell survival, Nat. Commun. 8 (2017) 14689, https://doi.org/10.1038/ncomms14689.

[60] D. Cao, X. Song, L. Che, X. Li, M.G. Pilo, G. Vidili, A. Porcu, A. Solinas, A. Cigliano, G.M. Pes, S. Ribback, F. Dombrowski, X. Chen, L. Li, D.F. Calvisi, Both de novo synthetized and exogenous fatty acids support the growth of hepatocellular carcinoma cells, Liver Int. 37 (2017) 80–89, https://doi.org/10.1111/liv.13183.

[61] J.J. Kamphorst, J.R. Cross, J. Fan, E. de Stanchina, R. Mathew, E.P. White, C. B. Thompson, J.D. Rabinowitz, Hypoxic and *Ras*-transformed cells support growth by scavenging unsaturated fatty acids from lysophospholipids, Proc. Natl. Acad. Sci. USA 11 (2013) 8882–8887, https://doi.org/10.1073/pnas.1307237110.

[62] A. Nath, I. Li, L.R. Roberts, C. Chan, Elevated free fatty acid uptake via CD36 promotes epithelial-mesenchymal transition in hepatocellular carcinoma, Sci. Rep. 5 (2015) 14752, https://doi.org/10.1038/srep14752.

[63] X. Luo, E. Zheng, L. Wei, H. Zeng, H. Qin, X. Zhang, M. Liao, L. Chen, L. Zhao, X. Z. Ruan, P. Yang, Y. Chen, The fatty acid receptor CD36 promotes HCC progression through activating Src/PI3K/AKT axis-dependent aerobic glycolysis, Cell Death Dis. 12 (2021) 328, https://doi.org/10.1038/s41419-021-03596-w.

[64] S. Softic, D.E. Cohen, C.R. Kahn, Role of dietary fructose and hepatic de novo lipogenesis in fatty liver disease, Dig. Dis. Sci. 61 (2016) 1282–1293, https://doi.org/10.1007/s10620-016-4054-0.

[65] P.J. Jones, A.S. Pappu, L. Hatcher, Z.C. Li, D.R. Illingworth, W.E. Connor, Dietary cholesterol feeding suppresses human cholesterol synthesis measured by deuterium incorporation and urinary mevalonic acid levels, Arterioscler. Thromb. Vasc. Biol. 16 (1996) 1222–1228, https://doi.org/10.1161/01.atv.16.10.1222.

[66] G.N. Ioannou, C.S. Landis, G.Y. Jin, W.G. Haigh, G.C. Farrell, R. Kuver, S.P. Lee, C. Savard, Cholesterol crystals in hepatocyte lipid droplets are strongly associated with human nonalcoholic steatohepatitis, Hepatol. Commun. 3 (2019) 776–791, https://doi.org/10.1002/hep4.1348.

[67] G.C. Farrell, F. Haczeyni, S. Chitturi, Pathogenesis of NASH: how metabolic complications of overnutrition favour lipotoxicity and pro-inflammatory fatty liver disease, Adv. Exp. Med. Biol. 1061 (2018) 19–44, https://doi.org/10.1007/978-981-10-8684-7_3.

[68] V.T. Samuel, G.I. Shulman, Nonalcoholic fatty liver disease as a nexus of metabolic and hepatic diseases, Cell Metab. 27 (2018) 22–41, https://doi.org/10.1016/j.cmet.2017.08.002.

[69] E.M. Griner, M.G. Kazanietz, Protein kinase C and other diacylglycerol effectors in cancer, Nat. Rev. Cancer 7 (2007) 281–294, https://doi.org/10.1038/nrc2110.

[70] D.L. Gorden, P.T. Ivanova, D.S. Myers, J.O. McIntyre, M.N. VanSaun, J.K. Wright, L.M. Matrisian, H.A. Brown, Increased diacylglycerols characterize hepatic lipid changes in progression of human nonalcoholic fatty liver disease; comparison to a murine model, PLoS One 6 (2011) e22775, https://doi.org/10.1371/journal.pone.0022775.

[71] E.M. Deacon, T.R. Pettitt, P. Webb, T. Cross, H. Chahal, M.J. Wakelam, J.M. Lord, Generation of diacylglycerol molecular species through the cell cycle: a role for 1-stearoyl, 2-arachidonyl glycerol in the activation of nuclear protein kinase C-betaII at G2/M, J. Cell Sci. 115 (2002) 983–989, https://doi.org/10.1242/jcs.115.5.983.

[72] S. Cases, S.J. Stone, P. Zhou, E. Yen, B. Tow, K.D. Lardizabal, T. Voelker, R. V. Farese Jr., Cloning of DGAT2, a second mammalian diacylglycerol acyltransferase, and related family members, J. Biol. Chem. 276 (2001) 38870–38876, https://doi.org/10.1074/jbc.M106219200.

[73] L.L. Listenberger, X. Han, S.E. Lewis, S. Cases, R.V. Farese Jr., D.S. Ory, J. E. Schaffer, Triglyceride accumulation protects against fatty acid-induced lipotoxicity, Proc. Natl. Acad. Sci. USA 100 (2003) 3077–3082, https://doi.org/10.1073/pnas.0630588100.

[74] K.N. Rao, M.F. Melhem, H.F. Gabriel, E.D. Eskander, M.E. Kazanecki, J.S. Amenta, Lipid composition and de novo cholesterogenesis in normal and neoplastic rat mammary tissues, J. Natl. Cancer Inst. 80 (1988) 1248–1253, https://doi.org/10.1093/jnci/80.15.1248.

[75] M. Régnier, A. Polizzi, H. Guillou, N. Loiseau, Sphingolipid metabolism in non-alcoholic fatty liver diseases, Biochimie 159 (2019) 9–22, https://doi.org/10.1016/j.biochi.2018.07.021.

[76] O. Vvedenskaya, T.D. Rose, O. Knittelfelder, A. Palladini, J.A.H. Wodke, K. Schuhmann, J.M. Ackerman, Y. Wang, C. Has, M. Brosch, V.R. Thangapandi, S. Buch, T. Züllig, J. Hartler, H.C. Köfeler, C. Röcken, Ü. Coskun, E. Klipp, W. von Schoenfels, J. Gross, C. Schafmayer, J. Hampe, J.K. Pauling, A. Shevchenko, Nonalcoholic fatty liver disease stratification by liver lipidomics, J. Lipid Res. 62 (2021) 100104, https://doi.org/10.1016/j.jlr.2021.100104.

[77] B. Babiy, B. Ramos-Molina, L. Ocaña, S. Sacristán, D. Burgos-Santamaría, J. Martínez-Botas, R. Busto, C. Perna, M.D. Frutos, A. Albillos, Ó. Pastor, Dihydrosphingolipids are associated with steatosis and increased fibrosis damage in non-alcoholic fatty liver disease, Biochim. Biophys. Acta Mol. Cell Biol. Lipids 1868 (2023) 159318, https://doi.org/10.1016/j.bbalip.2023.159318.

[78] S.J. Zheng, F. Qu, J.F. Li, J. Zhao, J.Y. Zhang, M. Liu, F. Ren, Y. Chen, J.L. Zhang, Z. P. Duan, Serum sphingomyelin has potential to reflect hepatic injury in chronic hepatitis B virus infection, Int. J. Infect. Dis. 33 (2015) 149–155, https://doi.org/10.1016/j.ijid.2015.01.020.

[79] A. Prola, F. Pilot-Storck, Cardiolipin alterations during obesity: exploring therapeutic opportunities, Biology 11 (2022) 1638, https://doi.org/10.3390/biology11111638.

[80] K.Y. Peng, M.J. Watt, S. Rensen, J.W. Greve, K. Huynh, K.S. Jayawardana, P. J. Meikle, R.C.R. Meex, Mitochondrial dysfunction-related lipid changes occur in nonalcoholic fatty liver disease progression, J. Lipid Res. 59 (2018) 1977–1986, https://doi.org/10.1194/jlr.M085613.

[81] P. Jha, M.T. McDevitt, R. Gupta, P.M. Quiros, E.G. Williams, K. Gariani, M. B. Sleiman, L. Diserens, A. Jochem, A. Ulbrich, J.J. Coon, J. Auwerx, D. J. Pagliarini, Systems analyses reveal physiological roles and genetic regulators of liver lipid species, Cell Syst. 6 (2018) 722–733, e6, https://doi.org/10.1016/j.cels.2018.05.016.

[82] M. Aoun, G. Fouret, F. Michel, B. Bonafos, J. Ramos, J.P. Cristol, M.A. Carbonneau, C. Coudray, C. Feillet-Coudray, Dietary fatty acids modulate liver mitochondrial cardiolipin content and its fatty acid composition in rats with non alcoholic fatty liver disease, J. Bioenerg. Biomembr. 44 (2012) 439–452, https://doi.org/10.1007/s10863-012-9448-x.